

Clinical and Genetic Characterization of Polydactyly in Selected Families



By

Arooba Nazir

Department of Biochemistry
Faculty of Biological Sciences
Quaid-i-Azam University Islamabad, Pakistan
2024

Clinical and Genetic Characterization of Polydactyly in Selected Families



A thesis submitted in partial fulfillment of the requirements for the degree of Master
of Philosophy

in

Biochemistry/Molecular Biology

by

Arooba Nazir

Department of Biochemistry
Faculty of Biological Sciences
Quaid-i-Azam University Islamabad, Pakistan
2024

My parents and brother have always been my source of inspiration. This thesis is dedicated to them For Their Endless Love, Encouragement, And Prayers.

Quaid-i-Azam University, Islamabad, PAKISTAN
Department of Biochemistry
Faculty of Biological Sciences

CERTIFICATE


This thesis, submitted by **Ms. Arooba Nazir** to the Department of Biochemistry, Faculty of Biological Sciences, Quaid-i-Azam University, Islamabad, Pakistan, is accepted in its present form as satisfying the thesis requirement for the Degree of Master of Philosophy in Biochemistry/Molecular Biology.

Examination Committee:


1. **External Examiner:**

Signature: _____

2. **Supervisor:**
Prof. Dr. Wasim Ahmad

Signature: _____ 

3. **Chairperson:**
Prof. Dr. Iram Murtaza

Signature: _____ 

Dated:

Declaration

I hereby declare that the work presented in this thesis is my effort and hard work. It is written and composed by me. No part of this thesis has been previously published or presented for any other degree or certificate.

Arooba Nazir

Table of Content

Acknowledgments	iv
LIST OF FIGURES	vi
LIST OF TABLES	viii
LIST OF ABBREVIATIONS	ix
ABSTRACT	xi
Human Skeleton	1
Bone and its Morphology	1
Bone Remodeling	2
Categories of Bones	2
Cartilage	3
Skeletal Patterning	5
Axial Skeleton	5
Appendicular Skeleton	6
Craniofacial Skeleton	7
Skeletal Pathways	7
Wnt Signaling Pathway	7
Hedgehog Signaling Pathway	8
BMP Signaling Pathway	9
FGF Signaling Pathway	10
Notch Signaling Pathway	10
Genetic Skeletal Dysplasia	11
Polydactyly	12
Genetic Classification of Polydactyly	13
Syndromic Polydactyly	13
Ellis-Van Crevald (EVC) Syndrome	14
Non-syndromic Polydactyly	15
I. Radial or Pre-axial Polydactyly (PPD)	15
i. Pre-axial Polydactyly type 1 (PPD1)	16
ii. Pre-axial Polydactyly type 2 (PPD2)	16
iii. Pre-axial Polydactyly type 3 (PPD3)	17
iv. Pre-axial Polydactyly type 4 (PPD4)	17
II. Ulnar or Post-axial Polydactyly	18
1. Post-axial Polydactyly type A (PAPA)	19
2. Postaxial Polydactyly type B (PAPB)	24

III. Complex Polydactyly	25
i. Mesoaxial or Central Polydactyly	25
ii. Mirror-Image Polydactyly (MIP)	25
iii. Palmer and Dorsal Polydactyly	26
iv. Haas Type Polysyndactyly	26
Aims and Objectives	26
Study Subjects and Ethical Approval	28
Pedigree Construction	28
Blood Sample Collection	28
Genomic DNA Extraction	28
Extraction of Genomic DNA by Phenol-Chloroform Method	29
Day 1st	29
Day 2nd	29
Extraction of Genomic DNA by Kit Method	30
Agarose Gel Electrophoresis (1%)	31
DNA Quantification and Dilution	32
Genotyping	32
Polymerase Chain Reaction (PCR)	32
Polyacrylamide Gel electrophoresis (Vertical Gel)	33
Whole Exome Sequencing (WES)	34
Primer Designing	35
Pre-sequencing PCR	35
Agarose Gel (2%)	36
Purification of Amplified PCR Product	36
Sanger Sequencing Analysis	37
RESULTS	41
Families Description	41
Family A	41
Clinical Features	41
Genetic Investigations	41
Family B	42
Clinical Features	42
Genotyping and Linkage Analysis in Family B	42
REFERENCES	57

Acknowledgments

All praises and glories to Almighty “**ALLAH**” who says in the Holy Quran, “And your Lord is the most gracious who taught by the pen. Taught man (those things) which he did not know”. Countless Darood on the Prophet **HAZRAT MUHAMMAD (Sall-Allah-Ho-Alaihay-Wa-Aalayhi-Wasallam)**, who showed the path of knowledge to mankind and gave the lessons of seeking knowledge from cradle to the grave.

I am greatly honored to pay my deep gratitude to my most learned, and considerate supervisor **Prof. Dr. Wasim Ahmad**, Department of Biochemistry, Faculty of Biological Sciences, Quaid-I-Azam University Islamabad, under whose inspiring guidance, and encouragement this research work was carried out. Without his support and kind efforts this task would have been impossible. I’m thankful to **Dr. Irum Murtaza** Chairperson, Department of Biochemistry, for her dedication to thriving the research activities in the department. I want to express my gratitude to **Dr. Imran Ullah**, Assistant Professor for helping and guiding us with the research activities in the laboratory.

I wish to express sincere thanks to my worthy seniors **Mr. Fatih Ullah, Kifayat Ullah, Hajira Fayyaz** and for their cooperation, and suggestions which have had a great impact on my research work, and Without their help, my work would be difficult. I express my gratitude to **Dr. Hammal Khan Zehri** and **Dr. Abdullah** for their unwavering guidance and support throughout my research. I must appreciate the friendly and cooperative attitude of my lab seniors **Dr. Attieya Zaman, Amjad Tanoli, Aamir Sohail, Inam Banochi, Tahir, Hamadia, Zumar Fatima, M. Ilyas, Palwasha Iqbal, Irum, Mirab, and Murtaza.**

I am extremely thankful to my classmates **Raza, Rehmat, Ayesha Sani, and Sher Aziz** for their moral support throughout my research journey. I am also thankful to my lab juniors **Naushaba Manan, Awais Haider, Sundus, and Hadiqa** for the respect they gave to me.

I sincerely thank my best friends **Aimen Farooq, Hafiza Ismail, and Sania Munir** for their company and prayers. I am extremely thankful to my classmates **Laiba, Faseeha, and Maria** for their constant moral support throughout my academic journey. I am also thankful to my seniors **Umer Khitab, and Mehreen** for their care, nice company, and support throughout university life.

I convey my heartiest thanks to the departmental clerical staff **Mr. Tariq Mehmood**, **Mr. Fayyaz**, and **Mr. Shehzad** for their sociable cooperation and sincere services towards students.

I must express my heartfelt gratitude to my family, with a special mention to my beloved mother **Sakina Nazir**, my father **Muhammad Nazir**, and my brother **M. Haroon Ali**. I also express my sincere thanks to my aunty **Nasreen Akhtar**. Their unwavering support, boundless encouragement, and well wishes have been the driving force behind my achievements.

Lastly, I extend a sincere acknowledgment to myself for maintaining unwavering self-belief during the most challenging phases of my academic journey. My tenacity and self-confidence have been pivotal in surmounting obstacles, making this journey of growth and learning more remarkable.

Arooba Nazir

LIST OF FIGURES

Figures	Title	Page number
Figure 1.1	Schematic diagram of different types of bone cells.	2
Figure 1.2	Describes membranous ossification and endochondral ossification.	4
Figure 1.3	Axial and appendicular views of the human skeleton are shown in this cartoon.	7
Figure 1.4	Wnt signaling pathway involved in skeletal pathways for maturation of osteoclasts.	8
Figure 1.5	Hedgehog signaling pathway involved in bone homeostasis.	9
Figure 1.6	FGF signaling pathway controls bone formation.	10
Figure 1.7	Modulation of osteocyte activity and osteoblast development by Notch pathway.	11
Figure 1.8	Representation of many forms of pre-axial polydactyly.	18
Figure 1.9(a)	Illustration of various types of post-axial polydactyly type A (PAPA) from type 1 to 4 in which the red color portrays the affected digit.	23
Figure 1.9(b)	Illustration of various types of post-axial polydactyly type A (PAPA) from type 5 to 8 in which the red color portrays the affected digit.	23
Figure 1.9(c)	Illustration of various types of post-axial polydactyly type A (PAPA) from type 9 to 11 in which the red color portrays the affected digit.	23
Figure 1.10	Illustration of Post-axial polydactyly Type B (PAPB) in which the red color portrays the affected digit.	25
Figure 1.11	Forms of complex polydactyly in which the red color portrays the affected digit.	26

Figure 3.1	Pedigree based on two generations of Family A identified with non-syndromic Polydactyly illustrating the autosomal recessive pattern of inheritance	45
Figure 3.2	A detailed overview of the clinical manifestations observed in the affected patients indicating phenotypes in family A	45
Figure 3.3	The pedigree of three generations in Family B identified with EVC syndrome illustrating the autosomal recessive pattern of inheritance	48
Figure 3.4	Comprehensive visuals of the clinical characteristics observed in the affected members of Family B	49
Figure 3.5	Results of the <i>GLI1</i> and <i>GLI3</i> flanking microsatellite markers in family B	51
Figure 3.6	Results of the <i>IQCE</i> and <i>DYNC2H1</i> flanking microsatellite markers in family B	52
Figure 3.7	Results of the <i>EVC</i> and <i>EVC2</i> flanking microsatellite markers in family B	53
Figure 3.8	Results of the <i>FAM92A1</i> and <i>MIPOL1</i> flanking microsatellite markers in family B	55

LIST OF TABLES

Tables	Title	Page number
Table 1.1	PDD Classification	18
Table 1.2	PAP Classification	23
Table 2.1	Description of solutions composition in DNA extraction protocol	31
Table 2.2	Description of solutions composition used in agarose gel electrophoresis	32
Table 2.3	PCR Components and their concentrations	33
Table 2.4	Details of Thermocycler conditions used for the PCR amplification of both families.	34
Table 2.5	Composition and Quantities of Solutions Used for the PAGE Preparation	35
Table 2.6	Primer sequences of the genes involved in Polydactyly	38
Table 2.7	List of Microsatellite Markers Used for Homozygosity Mapping	39
Table 3.1	Analysis of variants detected in exome data in family A	47

LIST OF ABBREVIATIONS

AD	Autosomal Dominant
AR	Autosomal Recessive
AMD	Acromesomelic Dysplasia
AER	Apical Ectodermal Ridge
BBS	Bardet-beidl Syndrome
BMP	Bone morphogenetic proteins
DLL3	Delta-like ligand 3
DNA	Deoxyribonuclease
DACH1	Dachshund Family Transcription Factor 1
EB	Elution Buffer
EDTA	Ethylene Diamine Tetraacetate
EtBr	Ethidium Bromide
EVC	Ellis-Van Creveld Syndrome
FGF	Fibroblast growing factor
FZD	Frizzled
GATK	Genome Analysis Tool kit
GCPS	Greig Cephalo-Polysyndactyly Syndrome
HEC	Higher Education Commission
HGMD	Human Genome Mutation Database
IQCE	IQ Motif containing E
IRB	Institutional Review Board
LDL	Low-density lipoproteins
LMBR1	Limb Development Membrane Protein 1
MSC	Mesenchymal stem cell

OD	Optical Density
PAP	Postaxial Polydactyly
PAP-A	Postaxial Polydactyly Type A
PAP-B	Postaxial Polydactyly Type B
PCR	Polymerase Chain Reaction
PPD	Preaxial Polydactyly
PHS	Pallister-Hall syndrome
Rpm	Rotation Per Minute
SCD	Spondylocostal dysostoses
SD	Skeletal dysplasia
SHFM	Split Hand and Foot Malformation
SHH	Sonic Hedgehog
SMO	Smoothened
SNV	Single Nucleotide Variant
TBE	Tris-Borate EDTA
TE	Tris EDTA Buffer
TGF- β	Transforming Growth Factor Beta
TPT	Tri-phalangeal Thumb
GLI3	Gli Family Zinc Finger 3
WB	Wash Buffer
WES	Whole Exome Sequencing
WNT	Wingless-type MMTV integration site family
YCGA	Yale Centre for Genome Analysis
ZNF	Zinc Finger Protein
ZPA	Zone of the Polarising Activity

ABSTRACT

Polydactyly, also known as hexadactyly or hyperdactyly, is a genetic limb disorder characterized by the presence of an extra digit. Polydactyly can be inherited in autosomal dominant (AD) or recessive (AR) form and has syndromic and non-syndromic types. Non-syndromic types are preaxial polydactyly (PPD) refers to an extra digit adjacent to the first digit on a radial side of the hand (thumb) or on a tibial side of the foot (toe). Postaxial polydactyly (PAP) refers to one or more additional digits at the ulnar/fibular side of the hand/foot. EVC syndrome is a type of Syndromic polydactyly and its characteristic features are post-axial polydactyly, leukonychia nails, dwarfism, dental and oral signs. Less variable symptoms of this syndromic polydactyly are post-axial polydactyly of feet and development retardation.

The current study investigated two consanguineous Pakistani families at clinical and genetic levels. Family A showed an autosomal recessive inheritance pattern of the disorder in the consanguineous family. Whole exome sequencing was performed on the affected members and several filters were applied to the exome data focused on pathogenic variants linked to non-syndromic polydactyly. Out of four selected variants, only two underwent segregation analysis but none of them segregated with the disorder. Therefore, it is recommended to conduct a segregation analysis with the other two variants.

Similarly, Family B was placed under the category of EVC syndrome. It showed an autosomal recessive inheritance pattern of the disorder. A search for the causative genes and variants was carried out using microsatellite markers to establish linkage in the family. Genotyping was performed using polymorphic microsatellite markers linked to eight candidate genes, including *GLI1* (12q13.3), *GLI3* (7p14.1), *DYNC2H1* (11q22.3), *IQCE* (7p22.3), *EVC1* (4p16.2), *EVC2* (4p16.2), *FAM92A* (8q22.1), *MIPOL1* (14q13.3). Genotyping failed to establish a linkage in the family to the tested markers. This indicated the involvement of novel genes causing the recorded phenotypes in the family.

INTRODUCTION

Human Skeleton

The skeleton system is a complex and evolutionary mechanism, composed of connective tissues, which is the extensive network of bones, ligaments, cartilage, and tendons. It comes from a variety of embryonic origins and serves essential functions. The primary role of the skeleton is movement and support in addition to its secondary function such as safeguarding the organs like the brain, spinal cord, lungs, heart, blood vessels, *etc* (Savarirayan and Rimoin, 2002). A research study has elucidated the multifaceted role of the skeletal system, positing its capacity to serve as an endocrine organ alongside its established role as the principal repository for mineral storage during postnatal development (Hartman, 2007). Except for the sesamoid bones, the skeletal system of a mature human is composed of 213 bones. The axial skeleton comprises a total of 74 bones, encompassing six auditory ossicles. The appendicular skeleton, on the other hand, comprises 126 bones, which include those of the hands, feet, upper and lower limbs, shoulder girdle, and pelvic bones (Ahmad *et al.*, 2022).

Bone and its Morphology

Bone is the most important connective tissue of the skeleton which plays a crucial function in mobility, soft tissue support, defense, mineral storage, and hosting microbes (Kini and Nandeesh, 2012; Florencio-Silva *et al.*, 2015). 10% of bone is naturally and continuously regenerated, making it a metabolizing organ. Bone consists of spongy bone (25%) and cortical or compact bone (75%; El-Ganzuri *et al.*, 2015). Bones contain four types of cells e.g. osteoclasts, osteoblasts, bone lining cells, and osteocytes (Florencio-Silva *et al.*, 2015).

Osteoblasts (mesenchymal cells) are present on the mineralized matrix surface and their function is to form new bones. Its primary function is to release type I collagen and along with that it also secretes vast amounts of non-collagen proteins. Osteoblasts release the osteoid as some different proteins to start the procedure of creating tissue from the bone. The most numerous and long-lasting cells are osteocytes. The osteocytes serve as mechanosensory cells that alert bone remodeling is necessary. The amounts of

hormones like estrogen and glucocorticoids that affect the osteocyte's ability to survive can be detected by these cells. Where no bone resorption nor bone production takes place, the outermost layers of bone are covered by inactive flat-shaped osteoblasts, which are the cells that make up the bone lining. The bone's state of health determines the secretory activity of the lining cells. Influenced by the number of aspects osteoclasts developed from mononuclear cells of the hematopoietic stem cell, these are polynucleated and terminally differentiated cells (El-Ganzuri *et al.*, 2015; Florencio-Silva *et al.*, 2015).

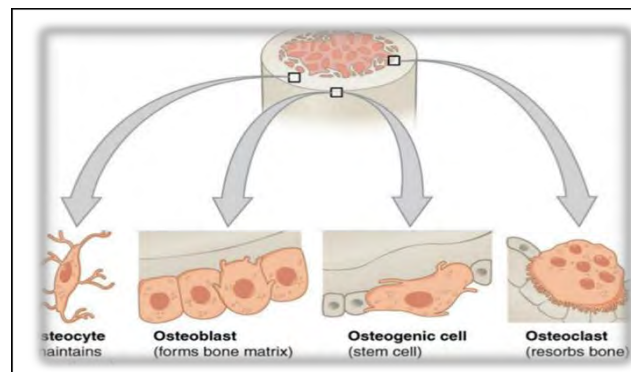


Figure 1. 1: Schematic diagram of different types of bone cells (El-Ganzuri *et al.*, 2015)

Bone Remodeling

During the active, growing, and developing years, the skeleton loses old bone and gains new bone, this continuous procedure is called bone remodeling. There are two phases of bone remodeling one is resorption, and the other is formation. In these phases, two cells are involved osteoclasts and osteoblasts. These cells perform a specific function in bone remodeling (El-Ganzuri *et al.*, 2015). In bone remodeling, the interaction between osteoblasts and osteoclasts occurs and abnormalities like small cracks get fixed because of this interaction. The process of resorption and formation are maintained in a homeostatic equilibrium such that fresh connective tissue is constantly replacing old bone. So bones adjust themselves to stress and pressure from the external environment (Hadjidakis and Androulakis, 2006).

Categories of Bones

Bones are classified into five distinct categories based on their morphological characteristics: namely, short, long, flat, irregular, and sesamoid bones.

A lengthy longitudinal direction characterizes long bones. Long bones serve as anchors to help muscles contract, supporting the body's weight and facilitating mobility. In addition to the femurs, radii, humeri, phalanges, ulnae, tibiae, metacarpals, clavicles, fibulae, and metatarsals, there are other long bones in the body. Short bones seem more cube-shaped and have a short horizontal axis. Tarsal bones and carpal bones are mainly short bones of the skeleton. They help with restricted movements and offer support as well as stability. These are spongy bones that help the ankle joint and wrist in movement. Flat bones are short and flexible, similar to numerous other bones in the skull. They protect the internal systems including the brain, lungs, heart, and liver, and provide a lot of space for muscle attachment. Flat bones consist of ribs, skulls, and mandibles. The dimensions and form of irregular bones vary and are frequently seen in clusters. Sacrum, vertebrae, and hyoid bones are irregular bones of the skeleton. During any stress or pressure condition internal organs like the spinal cord are protected by the vertebral column and the organ of the pelvic cavity is protected by the pelvis, both are irregular bones. The sesamoid bones are like sesame seeds because they mostly resemble these seeds. It is present in the ligaments of the hands, feet, and knees and protects the tendons from degeneration (Clarke, 2008; Forcica, 2014).

Cartilage

Cartilage is the connective tissue that performs a crucial function in the body. It assists the body in maintaining its shape and supports it (Caplan, 1984). Chondrocytes are the cells of the body that combine to form cartilage structures. At the time of birth, most bones are present in the form of cartilage but after the maturation period starts the cartilage is converted into mature bones but still some cartilage is present in its previous structure (Geister and Camper, 2015). The protein-containing component of cartilage is collagen. Different types of collagens are involved in the development of cartilage including collagens XI, IX, and II. Collagens X and collagens VI are two other types of proteins that are present in limited amounts in cartilage (Bruckner and Van Der Rest, 1994).

According to the physiological features, fibrous (*e.g.*, intervertebral disc), hyaline (*e.g.*, articular cartilage), and elastic (*e.g.*, ear cartilage) are three unique forms of cartilage (Lin and Klein, 2021). Where the ends of the bones are connected to form a joint, a

substance called hyaline cartilage is present. Its color is bluish-white, and its shape is glass-like thin. The elastic cartilage in the auricles of the ear is strong and has a yellow appearance. Ear cartilage, which also gives them flexibility and strength, maintains the shape of the ear. The disc between the vertebrae and the pubis symphysis contains fibrous cartilage, which is the third kind of cartilage, white in color, and has a high concentration of type I and type II collagen fibers (Hall, 2005).

Skeletal Development (Skeletogenesis)

Over 200 fragments of bone and cartilage are assembled into a framework during vertebrate skeletogenesis. At a specific spot in the body, every skeletal component is created (Lefebvre and Bhattaram, 2010). In the vertebrate embryo, skeletal development starts when multipotent mesenchymal cells develop from the ectoderm and mesoderm, leave to specific parts of the body and decide to become skeletal cells. During condensation, these mesenchymal cells split into chondrocytes (cartilage cells) and osteoblasts (bone cells). Skeletal development occurs in two processes, intramembranous ossification, and endochondral ossification.

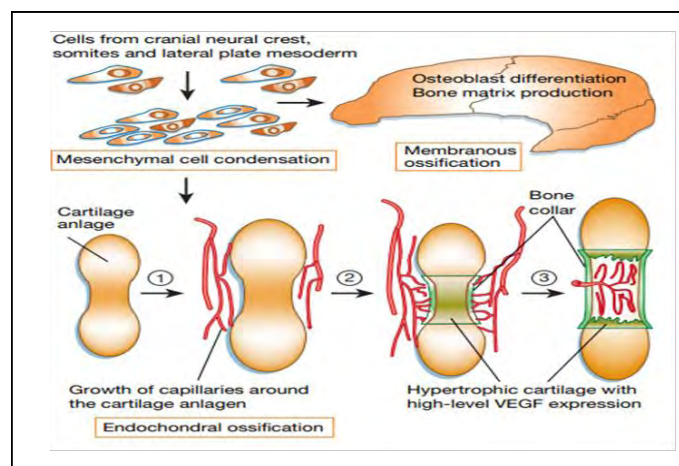


Figure 1.2: Membranous ossification and endochondral ossification. Firstly, aggregation of cells from the neural cranial crest occurs at the site where the formation of future bones occurs, and these cells form mesenchymal cell condensation. During intramembranous ossification, mesenchymal cells effectively differentiate into osteoblasts and produce the bone matrix. In endochondral ossification, the differentiation of cartilage and chondrocytes takes place first, and then these are replaced by bones. Capillaries formed around cartilage anlage in the first step. In the second step, cells around the anlage differentiate into osteoblasts, and chondrocytes in the center express large quantities of vascular endothelial growth factor (VEGF). The third

step involves forming growth plates and replacing hypertrophic cartilage with marrow (Zelzer and Olsen, 2003).

Skeletal Patterning

The dimension, form, number, and position of a vertebrate species' bones can be utilized to separate it from other vertebrate species; these characteristics are commonly referred to as skeletal patterns (Mariani and Martin, 2003). During a process known as pattern formation, skeletal identity acquires throughout early development before the mesenchymal condensation develops. Some of the primary processes that regulate the patterning are BMPs, FGFs, NOTCH/Delta, Wnts, and Hedgehogs (Franz-Odenaal, 2011). The axial skeleton, appendicular skeleton, and craniofacial skeleton give the origin of the skeleton (Kornak and Mundlos, 2003).

Axial Skeleton

Axial skeleton growth is a sequential activity that depends on complicated communication and well-coordinated cellular differentiation. All vertebrates have an axial skeleton that runs from anterior to posterior throughout the body axis and is made up of identical parts (Wellik, 2007; Williams *et al.*, 2019). The brain and spinal cord are supported and protected, while the skeletal muscles are anchored for mobility and stability (Mallo, 2020). It offers an outer layer for the joining of the muscles of the skeletal system that move the skull, neck, and upper body, assist breathing, and stabilize the proximal appendicular skeleton, including the forelimbs and hindlimbs, through the shoulders and pelvis girdles (Weldon and Munsterberg, 2022).

The axial skeleton, which is made up of the backbone and the dorsal section of the rib cage, is only partially derived from the somites, which are short-term ordering structures of the growing embryo located on both sides of the axial skeletal system. Blocks of epithelial cells with a sequential order make up somites, which develop from the paraxial mesoderm. The dermatomyotome is a structure that gives rise to the entire axial skeleton but firstly somites differentiate into dermatomyotome. The main origin of the axial skeleton is the sclerotome. (Kornak and Mundlos, 2003). “Spondylocostal dysostoses” (SCDs) affect the axial skeleton. *DLL3* variations lead to different kinds of dominant SCD, even though the origins of the bulk of these genetically diverse diseases are still unknown (Bulman *et al.*, 2000).

Appendicular Skeleton

An "appendage" is a prominent part of a vertebrate's body, and the adjective "appendicular" refers to this part of the body. The appendicular skeleton is composed of the upper as well as the lower limbs that attach to the axial skeleton at the joint between the shoulders and pelvis. The upper limbs contain 14 phalanges, 8 carpal bones, 5 metacarpals, 1 humerus, 1 shoulder girdle, 2 forearm bones (radius and ulna), and lower limbs contain 14 phalanges, 7 tarsal bones, 5 metatarsals, 1 femur, 1 coxal bone, and 2 leg bones (fibula and tibia). These are the bones that make up the appendicular skeletal system, and they are connected by an extensive amount of cartilage and joints. The appendicular skeleton's bones are crucial for the human body's ability to move and perform several other inclusive activities.

Many genes and pathways are involved in the development of the limbs. Not only gene families but the individual gene is involved in the limb's development. Abnormalities in genes and pathways cause limb malformation, syndromic and non-syndromic disorders. The final stages of the development of the limb buds are controlled by the apical ectodermal ridge (AER), the non-ridge ectoderm, and other established signaling systems including the ZPA (Zone of Polarizing Activity) (Ahmad *et al.*, 2022). Cell behavior involved in limb morphogenesis and outgrowth is controlled by Wnt5a and FGF signaling (Towers *et al.*, 2012).

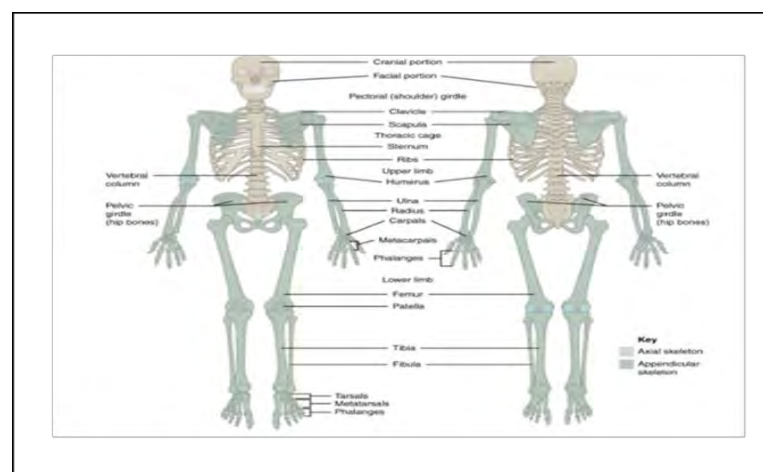


Figure 1.3: Green represents the appendicular skeleton and brown represents the axial skeleton (<https://philtschatz.com/anatomy-book/contents/m46374.html>).

Craniofacial Skeleton

One of the most identifying characteristics of humans is the structure of the face. The overall appearance of the human face and skull, the variety of facial features that people have, and the substantial heritability of facial features are basic biological and beneficial factors. Through these features, we examine the regulatory sequences of craniofacial morphology (Attanasio *et al.*, 2013). A craniofacial skeletal structure is complex, distinctive, and recognizable. The two main components of the craniofacial skeleton are the face bones, including the palatal, pharyngeal, temporal, and auditory bones known as viscerocranium, and the bones surrounding the brain (neurocranium). The entire viscerocranium and a portion of the neurocranium are derived from neural crest cells. To create the craniofacial skeleton, two different ossification methods are used. Some face bones, mandible, and most of the craniofacial bones, including the calvaria, are created through intramembranous ossification. On the other side, endochondral ossification creates the cranial base, which serves as a platform for the development of the brain. (Wilkie and Morriss-kay, 2001; Wei *et al.*, 2017).

The early fusion of one or more of the sutures in the cranium is known as cranial synostosis. The inherited mechanism for the disease is autosomal dominant. And in some cases, it's feasible for a syndromic gene to spontaneously change (Governale, 2015).

Skeletal Pathways

Wnt Signaling Pathway

Growth factors called Wnt proteins are secreted and are members of the conserved family of cysteine-rich glycoproteins. A wide range of cellular functions, including the development of organs during embryogenesis and maintaining the equilibrium of adult stem cells, depend on the pathways of signaling mediated by these ligands (Girardi and Le Grand, 2018). A 19-secreted protein family called Wnts that performs an essential function in several biological processes, Wnt binds to a combination of 10 frizzled membrane receptors. One of two low-density G-protein coupled receptors (FZD) and Lrps, also known as lipoprotein (LDL) receptor-related proteins. These several

intracellular communication subgroups are activated by binding processes depending on the cell types, Wnt, FZD, and Lrp involvement (Liu *et al.*, 2008).

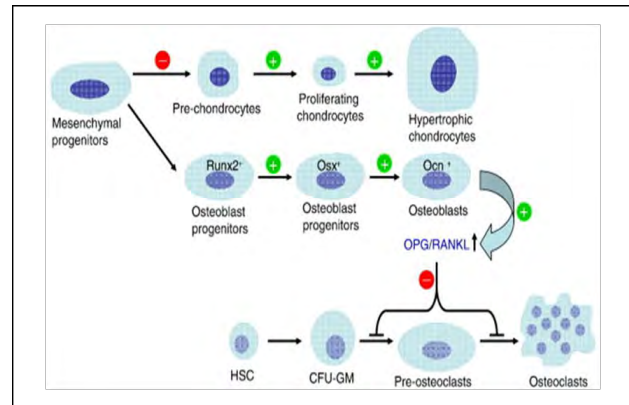


Figure 1.4: Function of canonical pathways in skeletal, according to external signals, mesenchymal stem cells can develop into chondrocytes or osteoblasts. This differentiation depends on canonical signaling, if the signal is weak then differentiation of mesenchymal cells into chondrocytes occurs. However, the maturation of chondrocytes needs a canonical signal. In the formation of osteoclasts, Wnt signaling is involved but sometimes the signal has a positive effect and sometimes harmful. Through a series of effects positive (green) and negative (red) the maturation of osteoclasts takes place (Liu *et al.*, 2008)

Hedgehog Signaling Pathway

Hedgehog signaling controls several cellular functions essential for bone growth. The GLI family of transcription factors, which are involved in the development, illness, and skeletal remodeling processes, are activated by the binding of hedgehog ligands to protein patched homologue 1 (PTC), a conserved receptor (Alman, 2015). Generated signaling molecules are essential for supplying positional knowledge and for defining cell destiny within an organ-forming embryo. During organ development and equilibrium, the cells reacting to these signals dramatically change the expression of their gene pathways and begin to carry out specific activities. Hedgehog signaling pathways can be classified into three categories: desert, Indian, and sonic. These three pathways perform different functions during the developmental process. The sonic hedgehog (SHH) and Indian hedgehog (IHH) are involved in the development of maturity of the skeletal components as well as the formation of most organs (Ehlen *et al.*, 2006).

SHH is the most critical HH pathway among all three pathways and it is mainly involved in the growth of the axial skeleton, limbs, brain, and spinal cord. During the

growth of long bones, IHH controls cartilage differentiation. DHH mainly impacts Schwann cells of the nervous system. Disruption in HH pathways causes diseases including post-axial polydactyly types 3, Holoprosencephaly, and Glioblastoma (Bale, 2002).

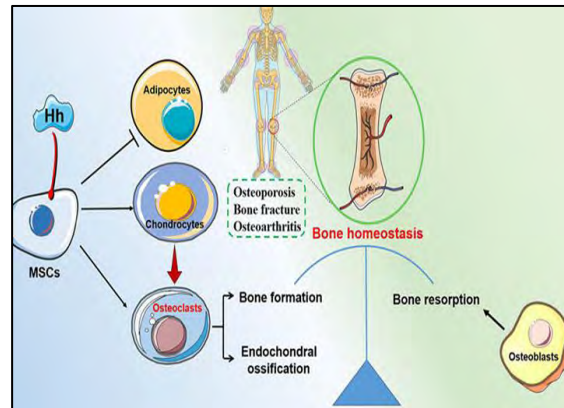


Figure 1.5: In controlling MSC differentiation and preserving bone homeostasis, hedgehog signaling is crucial. In contrast to promoting their differentiation into chondrocytes and osteoblasts, which are further involved in maintaining bone homeostasis where osteoblasts drive bone creation and osteoclasts control bone resorption, Hh signaling suppresses MSC differentiation into adipocytes. Osteoarthritis, osteoporosis, and bone fractures are among bone-related disorders that could be carried on by the instability of Hh signaling (Zhou *et al.*, 2022)

BMP Signaling Pathway

Participants of the TGF superfamily, bone morphogenetic proteins (BMPs) play important players in the signaling network and participate in all skeletal morphogenesis-related events. BMPs make up about one-third of the transforming growth factor- β (TGF- β), which was first discovered as a protein that promotes the production of bone and cartilage. The BMP signaling pathway is activated when many intracellular and extracellular proteins attach with the machinery of this signaling pathway and the transformation of the chemical messenger (signal) occurs from the cell membrane to the nucleus (Wan and Cao, 2005). Multiple BMPs, such as BMP-2, BMP-4, and BMP-7, cause multipotent mesenchymal cells to differentiate into osteochondrogenic lineage cells and osteoblast precursor cells. The important factor involved in osteoblasts differentiation is called BMP-2 (Yamaguchi *et al.*, 1996). Disruption in BMP signaling pathways causes many diseases including Osteoarthritis (OA), polydactyly, syndactyly, cancer, etc (Bandyopadhyay *et al.*, 2013).

FGF Signaling Pathway

FGF acts as a mitogen that controls the variety of biological functions in cells such as movement, growth, differentiation, proliferation, and maintenance (Xie *et al.*, 2020). FGF plays a very crucial role in both intramembranous and endochondral bone development. Early limb development, as well as the formation of the skeleton, depend on FGF signaling pathways (Ornitz and Marie, 2002). Fibroblast growth factors (FGFs) are crucial molecules that regulate the development of bones. FGF affects cells of the osteoblast lineage via activating FGF receptors (FGFRs) and downstream signaling cascades (Marie *et al.*, 2012). Craniosynostosis syndromes, chondrodysplasia, dwarfism syndromes, obesity, chronic kidney disease (CKD), insulin resistance, and skeletal overgrowth syndromes are caused by a Variation in *FGFR1*, 2, and 3 (Su, 2008).

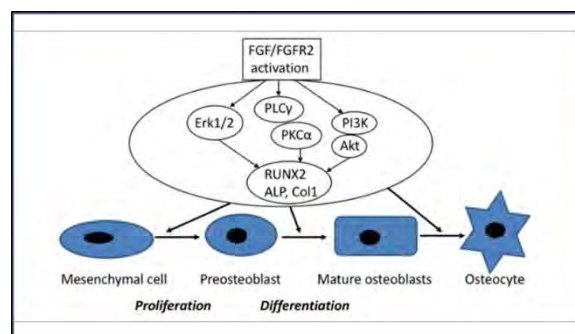


Figure 1.6: Fibroblast growth factor (FGF) and fibroblast growth factor receptor (FGFR) control bone formation. Osteoblastogenesis is mostly regulated by FGF/FGFR signaling, which also influences osteoblast differentiation and replication. The activation of ERK1/2 MAPK, PLC/PKC, and Akt activity results from the activation of FGF and FGFR and upregulates osteogenesis and osteoblast expression of genes (Kuroda *et al.*, 2019)

Notch Signaling Pathway

Notch signaling controls essential functions throughout embryonic growth and development, cell fate determination, differentiation, proliferation, and stability. Notch receptors and their ligands are proteins found in the membrane that physically involve cells to start the communication pathway. In humans four types of notch receptors (NOTCH1-4) contain five types of notch ligands (JAG1, JAG2, DLL1, DLL3, and DLL4) (Zieba *et al.*, 2020). A crucial modulator of the growth and renewal of skeletal

muscle is the Notch signaling system (Vargas-Franco *et al.*, 2022). Variations in many Notch network proteins are linked to Adams-Oliver syndrome (AOS), the protein component of this pathway is NOTCH1, DLL4. Almost all variations take place in NOTCH1 but some occur in other genes e.g., the Lack of *DLL4* function during AOS is caused by missense and nonsense variation in *DLL4* (Zieba *et al.*, 2020).

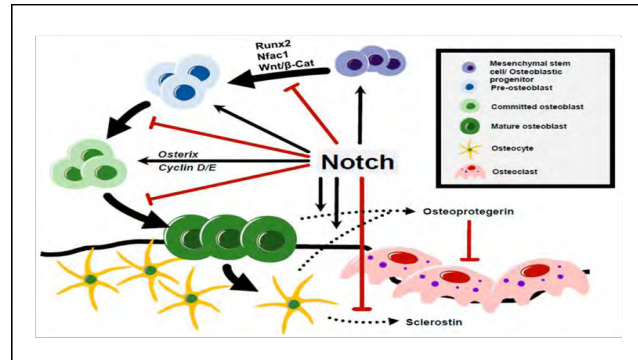


Figure 1.7: Modulation of osteocyte activity and osteoblast development by Notch pathway. By inhibiting the transformation of Runx2 and inhibiting osteoblast differentiation through Nfatc1-mediated reduction of Wnt/-catenin signaling to maintain the population of mesenchymal cells. By enhancing the transcription of Osterix, Cyclin D, and Cyclin E, Notch expression expands the number of premature osteoblasts. Osteoprotegerin activity by osteoblasts and osteocytes regulates bone resorption through Notch signaling. Notch activation in osteocytes also decreases sclerostin, enhancing Wnt signaling and preventing the breakdown of bone (Zieba *et al.*, 2020)

Genetic Skeletal Dysplasia

Skeletal dysplasias are a genetically complex group of disorders that impact the growth, maintenance, and development of the human skeleton. Skeletal dysplasia refers to generalized skeletal malformations that primarily affect bone (osteodysplasias) and cartilage (chondrodysplasias, hence also known as osteochondrodysplasias). The malformation of a single bone or group of bones is known as dysostoses. Genetic skeletal disorders are classified into either nonsyndromic (isolated) or syndromic (complex syndromes) forms and are inherited in autosomal dominant or recessive, X-linked, or de novo forms (Baldrige *et al.*, 2010; Abbas *et al.*, 2023). Osteodysplasias and dysostoses are two terms used to describe skeletal conditions caused by abnormalities in the bony component of the skeleton. Osteodysplasias disrupt bone mineralization and result in osteoporosis and osteopenia, whereas dysostoses only affect a single skeletal component and have a more limited impact. Dysostoses often

occur from abnormal skeletal patterning gene activation (Hurst *et al.*, 2005; Schramm *et al.*, 2009). Chondrodysplasias are skeletal malformations that often affect the whole appendicular skeleton and are brought on by disruption of the cartilaginous component of the skeleton. Chondrodysplasias were caused by changes in organogenesis-related genes (Mortier, 2001).

Skeletal dysplasia may result from irregularities in the major signaling networks (WNT, Notch, Hedgehog, TGF B, etc.) that are crucial to the evolution of the skeletal elements. Numerous skeletal dysplasia is caused by defects in bone production, homeostasis, and mineralization (Marzin and Cormier-Daire, 2020). Hand and foot patterning anomalies are common types of limb skeletal dysplasias such as osteogenesis imperfect (OI), acromesomelic dysplasia (AMD), split hand and foot malformation (SHFM), bardet-beidl syndrome (BBS), brachydactyly, camptodactyly, syndactyly, and polydactyly (Abbas *et al.*, 2023).

Polydactyly

Polydactyly, also referred to as hyperdactyly or hexadactyly. Polydactyly is made up of the terms “poly means many” and “dactylos means digits” (Kerchring, 1988). When there are extra fingers, feet, or any advanced doubling of digital components, it is referred to as polydactyly or polydactylism (Umair *et al.*, 2018). Polydactyly is the most frequent genetic condition of hands and feet (Kyriazis *et al.*, 2023). It is one of the most frequent genetic limb abnormalities detected instantly after the time of birth and it can appear to be an entire or partial duplication of digits. Males get this disease twice as frequently as females; its prevalence has been calculated to be 1.6-10.7/1000 in the overall population and 0.3-3.6/1000 in live births (Mellin, 1963; Castilla *et al.*, 1973). There are more chances of affecting the right hand as compared to the left hand, increased risks of the left foot being more impacted than the right, and upper limbs being more affected than the lower (Castilla *et al.*, 1973; Malik *et al.*, 2014). Based on research in the USA, the prevalence of polydactyly is 22 times higher in Black women than White women, and 10 times higher in Black men than White men. White males experience polydactyly at a rate of 2.3 per 1000, Black males at 13.5 per 1000, and White females at 0.6 per 1000, compared to 11.1 per 1000 for Black females (Finley *et al.*, 1994).

A flaw in limb growth and development, specifically in the arrangement of the growing limb buds on both posterior and anterior surfaces, results in polydactyly. Polydactyly is also produced from a variety of variables, such as hereditary and mutagenic ones that disrupt the molecular mechanisms of digit development. This condition exists in families and its most prevalent mode of inheritance is autosomal dominant. If the parents carry one allele of this disorder then a 50% probability is that each to inherit the disorder, which means both genders are affected equally (Farrugia and Calleja-Agius, 2016).

Genetic Classification of Polydactyly

Syndromic and non-syndromic polydactyly are the two broad-spectrum classifications of polydactyly. Pre-axial polydactyly (PPD) has an extra digit attached to the radial side of the hand *i.e.*, thumb side or tibial part of the foot *i.e.*, first toe, referred to as the anterior to median axis of the limb, and post-axial polydactyly (PAP) is distinguished by an extra digit at the fifth finger or toe forming the ulna aspect of the hand and fibular part of the foot respectively creating the posterior position to median axis of limbs, are the two predominant forms of polydactyly (Lange and Muller, 2017). On the contrary, meso-axial polydactyly, which includes the duplication of the second, third, or fourth digit, is an uncommon type of digit malformation (Umair *et al.*, 2018).

Syndromic Polydactyly

According to the London Dysmorphology database, there are 221 syndromic polydactylies and 120 syndromic oligodactyly illnesses. ‘8659’ entries appear on typing the word ‘Syndromic Polydactyly’ in the online OMIM database (<https://www.omim.org/>). The most reported digit abnormalities are Ellis- Van Creveld (EVC) Syndrome (OMIM 225500), Pallister-Hall Syndrome (OMIM 146510), Bardet-Biedl Syndrome (BBS) (OMIM 617119), and Greig Cephalopolysyndactyly Syndrome (OMIM 175700), Acrocephalosyndactyly, MuKusick-Kaufman Syndrome (OMIM 236700), Short rib polydactyly and Smith-lemli Optiz Syndrome (OMIM **270400**) (Ahmad *et al.*, 2023). Greig Cephalopolysyndactyly Syndrome appears in syndromic form with segregation in an autosomal dominant manner and usually refers to deformities of the head, face, and limb, whereas the latter typically has cutaneous

syndactyly and finger or toe polydactyly. Pallister- Hall Syndrome occurs in autosomal dominant inheritance and is characterized by a range of developmental defects such as cutaneous syndactyly and polydactyly. Bardet-Biedl Syndrome also has syndromic representation but in a recessive manner. Syndactyly and polydactyly in the fingers and toes are linked to Bardet-Biedl syndrome (BBS). The characteristics of acrocephalosyndactyly syndromes include polydactyly and syndactyly, as well as craniosynostosis. Two characteristics are associated with McKusick-Kaufman syndrome: polydactyly, genital abnormalities, and cardiac problems. There are two characteristics of short-rib polydactyly syndromes: preaxial polydactyly and a thin thorax. Multiple bodily areas are affected by Smith-Lemli-Opitz syndrome, whereas either the fingers or the toes are affected by polydactyly and the second and third toes are mainly affected by syndactyly (Ahmed *et al.*, 2017).

Ellis-Van Crevald (EVC) Syndrome

Ellis-Van Crevald Syndrome is categorized as ciliopathy and is included in the category of chondro-ectodermal dysplasia and is caused by variation at chromosome 4p16. It is a genetic disorder that segregates in an autosomal recessive manner. Characteristic features of Ellis-Van Crevald Syndrome (OMIM 225500) include post-axial polydactyly, cardiac problems, dental and oral signs, dwarfism, hypoplastic or dystrophic nails, and radiologic problems. Less frequent and variable symptoms of EVC are upper lips problems, post-axial polydactyly of feet, and retardation in development. The *EVC* gene on chromosome 4p16 and the *EVC2* gene, which is situated adjacent to the *EVC* gene in a competing arrangement, are mutated in this syndrome (Thomas *et al.*, 2022; Da Silva *et al.*, 2023). *EVC* gene contains 21 coding exons and produces 992 amino acid proteins while *EVC2* gene contains 22 coding exons and produces 1308 amino acid proteins (Ali *et al.*, 2010).

EVC and *EVC2* proteins located at the base of primary cilia are involved in the activation of proteins like Smoothed (SMO) and Glioma-associated oncogene homolog (GLI2). *EVC/EVC2* forms a complex with SMO and interacts with *IQCE/EF CAB7* thereby activating the Hh pathway which is involved in limb formation and bone growth. EVC syndrome results from the inactivation of

EVC/EVC2 which affects the signaling cascade and leads to a defective Hh signaling pathway (Thomas *et al.*, 2022; Bilal *et al.*, 2023).

Non-syndromic Polydactyly

The temtamy-McKusick scheme provided the most popular categorization for the non-syndromic form of polydactyly. Pre-axial polydactyly (radial), complex types of polydactylies, and postaxial polydactyly (ulnar) are three broadly distinguished main sub-types of non-syndromic polydactyly (Temtamy and MuKusick, 1978). A minimum of ten locus and six genes, including the *EFCAB7*, *LRP4*, *KIAA0825*, *STKD1*, *DACHI*, and *FAM92A1* cause nonsyndromic polydactyly in humans (Umair *et al.*, 2018).

Recently two genes, *LRP4* and *EFCAB7* with variations leading to polydactyly have been reported. *LRP4* localized at chromosome 11 results in pre-axial polydactyly in feet and complex polydactyly due to heterozygous missense variants [c.1696G>A; p.(Gly566Ser)] in this gene. Post-axial polydactyly caused by two novel homozygous frameshift deletion [c.830delG; p.(Gly277Valfs*5)], [c.1350_1351delGA; p.(Asn451Phefs*2)] in *EFCAB7* have also been documented (Bilal *et al.*, 2023; Khan *et al.*, 2023).

I. Radial or Pre-axial Polydactyly (PPD)

The radial side of the hand may exhibit polydactyly, which is defined as the duplication or incomplete separation of a finger during development. Preaxial polydactyly may be associated with duplication of metacarpal and phalangeal segments. It is sometimes referred to as radial polydactyly, split thumb, or thumb duplication. Preaxial polydactyly frequently arises from the absence of differentiation and a failure of development that affects the hand plate's anterior-posterior development path. The zone of polarizing activity (ZPA), a particular communication center, is found in this region and is situated in the back of the growing bud. The SHH signaling protein, which the ZPA produces, and SHH signaling proteins are involved in limb development so when disruption occurs in this signaling protein it leads to the preaxial polydactyly (Rogers *et al.*, 2020).

Preaxial polydactyly (PPD), which occurs between 0.08% and 1.4% of the time for every 1000 live births, is not as common as PAP. Duplications of all kinds, from a

typical thumb to a completely duplicated ray, can occur in PPD. Pre-axial polydactyly has four subtypes (Temtam and McKusick, 1978).

i. Pre-axial Polydactyly type 1 (PPD1)

One or more skeletal parts of a bi-phalangeal thumb were duplicated, which was described as preaxial polydactyly Type I (Orioli and Castilla, 1999). The most prevalent kind of thumb polydactyly is the duplication of a bi-phalangeal thumb. The condition is typically unidirectional, but in bidirectional situations, hands are more frequently suffering and left-hand PPD is less common than right-hand PPD (Malik *et al.*, 2014; Umair *et al.*, 2018). PPD type I contains a pattern of autosomal dominant inheritance and low penetration, which means PPD type I is a rare disorder (Castilla *et al.*, 1973; Orioli and Castilla, 1999; Burger *et al.*, 2018). This disorder is less common in females than males (Orioli and Castilla, 1999). The regulatory sequence of the sonic hedgehog (SHH) enhancers is called the zone of polarizing activity (ZPA). Variation in ZPA causes PPD type I disorder (Lettice *et al.*, 2002; Wieczorek *et al.*, 2010; Perez-Lopez *et al.*, 2018). Another type of thumb polydactyly (PPD type I) is hallux polydactyly. It is understood that it can occur in populations as a dominant expression. As compared to the ratio between males and females, males are more affected (Castilla *et al.*, 1973; Orioli and Castilla, 1999). Hallux polydactyly produced when micro or small deletion occurs at chromosome 2q31.1-31.2 (Tsai *et al.*, 2009).

ii. Pre-axial Polydactyly type 2 (PPD2)

Polydactyly is a common disorder nowadays but as compared to other forms, type II preaxial polydactyly is rare (Thioritz *et al.*, 2019). Preaxial polydactyly type 2 is characterized by the first metacarpal being excessively thin and lengthy, with spines on each of its ends, and the thumb possesses an additional intermediate bone. PPD type II has been discovered to be transmitted dominantly with intermediate penetration on chromosome 7q36 (Temtam and McKusick, 1978; Tsukurov *et al.*, 1994; Umair *et al.*, 2018). The PPD type 2 disease is caused by ZRS located in the *LMBR1* gene's intron 5 (Lettice *et al.*, 2003).

iii. Pre-axial Polydactyly type 3 (PPD3)

It contains an extra middle finger and an autosomal dominant pattern of inheritance. And uncommon polydactyly disorder (Malik, 2014). It has a malformation of the fingers, replacing the thumb with one or two triphalangeal digits that have an index finger-specific dermatoglyphic pattern. Both bilaterally and unilaterally are possible (Atasu, 1976). Multiple investigations indicate that preaxial polydactyly type III is caused by a gene occurring on chromosome 7q36 (Perez-Lopez *et al.*, 2018). Although it has been additionally suggested that index polydactyly is a kind of thumb duplication, the terms "central polydactyly" and "index polydactyly" are frequently combined (Wood, 1970).

iv. Pre-axial Polydactyly type 4 (PPD4)

The thumb is only minimally copied, and the distal phalanxes indicate radial deformation or have a broad as well as bifid thumb (Bubshait, 2022). Third and fourth finger syndactyly can also arise in this form occasionally. The initial metacarpal on the primary bottom of the feet is short enough and the tibia is bent t (Temtamy and McKusick, 1978; Burger *et al.*, 2018).

The term "CP" is often used to describe the presence of preaxial polydactyly and post-axial polydactyly, with the main difference being the extra fingers on the axis of the hands and feet. In CP type 1 PAP in the hands and PPD in the feet are the most common symptoms, while PAP of the feet is shown along with PPD of the hands in CP type 2 (Temtamy and McKusick, 1978). This kind of polydactyly has been scientifically associated with *GLI3* genetic variations and ZRS locus (Radhakrishna *et al.*, 1999; Perez-Lopez *et al.*, 2018).

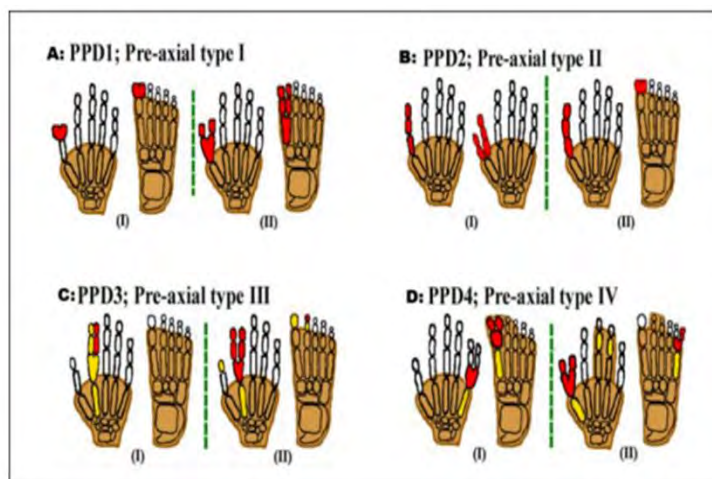


Figure 1.8: Different types of pre-axial polydactyly. **(A):** Pre-axial polydactyly type 1 (PPD1) has a common representation of a bi-phalangeal thumb either in the hand or feet as intimated in red, **(B):** Pre-axial polydactyly type 2 (PPD2) represents the tri-phalangeal thumb as shown in red, **(C):** Pre-axial polydactyly type 3 (PPD3) has the second finger with the distinctive dermatoglyphic pattern denoted in red, **(D):** Pre-axial polydactyly type 4 (PPD4) as indicated in red denotes the mildest degree of duplication which includes webbed/ connected fingers or toes (Umair *et al.*, 2018)

Table 1.1: PPD Classification.

Phenotype	OMIM ID	Locus	Genes	Inheritance
PPD1	165220	12q13.3	<i>GLI1</i>	AR
PPD2	174500	7q36.3	<i>LMPRI</i>	AD
PPD3	174600	U	<i>U</i>	AD
PPD4	174200	7p14.1	<i>GLI3</i>	AD

U: unknown, AD: autosomal dominant, AR: autosomal recessive

II. Ulnar or Post-axial Polydactyly

Another name of postaxial polydactyly is called ulnar polydactyly, A genetic condition of the upper limb has been defined by the development of an additional finger on the ulnar or fibular side of the hand at birth. These additional fibular or ulnar digits can be found along the fifth finger in postaxial polydactyly (Samarendra *et al.*, 2022). It is sometimes possible that the only clinical observation is a tiny tissue outgrowth or scar mark located near the proximal interphalangeal split. When comparing the ratio between preaxial and postaxial polydactyly, preaxial polydactyly (25%) is less common

than postaxial polydactyly (75%). Bilateral PAP in the lower as well as upper limbs affects about 8% of cases, and this condition is commonly accompanied by other genetic disorders (Verma and El-Harouni, 2015). Usually occurs in 1-2/1000 births that occur alive (Zhou *et al.*, 2004). According to the Stelling and Turek classification, there are three types of postaxial polydactyly, Soft-tissue duplication is present in type 1, osseous duplication is present in type 2, and a wholly duplicated ray, including the metacarpal, is present in type 3 (Comer *et al.*, 2018).

There are two categories of PAP according to Temtamy and McKusick, postaxial type A, and postaxial type B. Both have a difference in seriousness, hereditary arrangement, and penetration of prediction. In human genes involved in this polydactyly are *GLI3*, *GLI1*, *ZNF141*, *MIPOL1*, and *PITX1* (Malik, 2014; Umair *et al.*, 2018)

1. Post-axial Polydactyly type A (PAPA)

When it comes to PAP type A, an entirely formed additional digit is expressed depending on the fifth metatarsal or metacarpal or a duplicated metatarsal or metacarpal (Temtamy and McKusick, 1978). In daily life, in most cases, individuals face difficult situations due to additional digits. These additional digits show non-functional behavior. PAP type A contains low penetrance, and its segregation contains autosomal dominant traits (Castilla *et al.*, 1997; Kucheria *et al.*, 1981). PAP type A is present in 1-2/1000 births that are alive. PAP type A has either an autosomal dominant or autosomal recessive inheritance pattern on the ulnar or fibular side (Ahmad *et al.*, 2023).

PAP type A is divided into 11 subtypes (PAPA1 – PAPA11). When variations occur in these genes (*EFCAB7*, *ZNF141*, *IQCE*, *GLI1*, *FAM92A*, *GLI3*, *KIAA0825*, and *DACHI*) it leads to causing postaxial polydactyly subtypes disorder (Ahmad *et al.*, 2023).

i. Post-axial Polydactyly type A1 (PAPA1)

The fifth metacarpal has an effective additional finger and is caused by heterozygous variation in the *GLI3* gene (OMIM 165240) on chromosome 7p14.1 that is autosomal dominantly inherited (Umair *et al.*, 2018; Rahim *et al.*, 2020). Genetic testing revealed a heterozygous variation in the *GLI3* gene that is expected to cause premature

termination and may contribute to nonsense-mediated mRNA degradation. There have been 330 *GLI3* genetic variations documented that are linked to different skeletal disorders (Furniss *et al.*, 2007; Ahmad *et al.*, 2023).

ii. Post-axial Polydactyly type A2 (PAPA2)

This type of polydactyly contains an autosomal dominant pattern, and it is localized at chromosome 13q21-q32. Physical characteristics or symptoms of this form of the disorder are like those of PAPA1 (Rahim *et al.*, 2020). PAPA2 is characterized by the development of either unilateral or bilateral postaxial polydactyly. PAPA2 is still associated with an unidentified gene (van der Zwaag *et al.*, 2010; Kannu *et al.*, 2013).

iii. Post-axial Polydactyly type A3 (PAPA3)

In this kind of polydactyly, the additional finger on the hands and feet is fully grown. There are a variety of types with either one or both sets of digits. It contains an autosomal dominant pattern (Rahim *et al.*, 2020). The disease loci for PAPA3 were located at chromosomal regions 19p13.2-p13.1 using markers D19S1165 and D19S929 to identify the disorder. The gene responsible for the condition is still unknown (Ahmad *et al.*, 2023).

iv. Post-axial Polydactyly type A4 (PAPA4)

This disorder is similar to PAPA1. A properly formed additional digit expresses with the fifth or sixth metacarpal (Lange and Muller, 2017). PAPA4 was described in a six-generation Dutch community with an overall number of 31 members, 11 affected and 20 unaffected. PAPA4 has an inheritance with an autosomal dominant pattern (Galjaard *et al.*, 2003). PAPA4 is located on chromosome 7q22.1, exhibits autosomal dominant inheritance, and lacks a known pathogenic gene (Umair *et al.*, 2018).

v. Post-axial Polydactyly type A5 (PAPA5)

It is distinguished by five to six metacarpal synostoses, moderate syndactyly, and polydactyly of the hands and feet. This kind of autosomal recessive postaxial polydactyly has been seen in two Indian families and one Sicilian family. The 13q13.3–13q21.2 area was identified as the location of postaxial polydactyly type A5. This

phenotype's causative gene has not yet been discovered (Mohan, 1969; Kyriazis *et al.*, 2023).

vi. Post-axial Polydactyly type A6 (PAPA6)

An inheritance with an autosomal recessive pattern was seen in PAPA6. The fifth finger's terminal digit may also be duplicated in certain cases, and the affected individuals are distinguished by an extensive bilateral, properly formed duplicated fifth digit that is twisted towards the ulnar or the radial side (Ahmad *et al.*, 2023). Variants in the zinc finger *ZNF141* gene lead to cause PAPA6, which is found on chromosome 4p16.3 (Kucheria *et al.*, 1981).

vii. Post-axial Polydactyly type A7 (PAPA7)

This polydactyly was identified as having lower body parts with established nails. This kind has an autosomal recessive pattern of inheritance (Rahim *et al.*, 2020). Postaxial polydactyly type A7 is linked to *IQCE* diminished function. A 695-amino-acid protein produced by the *IQCE* gene positively controls the Hedgehog signaling pathway and is placed on chromosome 7p22.3. Polydactyly traits linked to aberrant Hh signaling have been reported to result from variations in the *IQCE* (Umair *et al.*, 2017; Tilemis *et al.*, 2023).

viii. Post-axial Polydactyly type A8 (PAPA8)

In addition to polydactyly, PAPA related to *EVC* also has phenotypes of atrial septal abnormalities, moderate nail malformations, low height, and genu valgum. Ellis-van Creveld syndrome (EVC), a condition characterized by reduced Hh signaling, existed together with these developmental abnormalities. According to reports, the *GLII* gene causes PAPA-EVC (Palencia-Campos *et al.*, 2017). PAPA8 has been linked to multiple unique variants in the *GLII* gene. A novel bi-allelic variation in exon nine of *GLII* [c.1010C > T; p.(Ser337Leu)] cause PAPA8 (Umair *et al.*, 2021).

ix. Post-axial Polydactyly type A9 (PAPA9)

Non-syndromic postaxial polydactyly in the upper, as well as the lower limbs, is a feature of PAPA9. The homozygous variations of the *FAM92A* gene, which is found on chromosome 8q21.13-q24.12, are linked to this autosomal recessive disease. PAPA9

was found to be linked to a single homozygous nonsense variation in the *FAM92A* (Schrauwen *et al.*, 2019).

x. Post-axial Polydactyly type A10 (PAPA10)

The *KIAA0825* gene, which is localized on chromosome 5q15, contains bi-allelic missense variants that were found in two Pakistani closely related families presenting PAPA10 unique traits. Six affected individuals from these two families are characterized by traits including established fifth digit duplication in the hands and feet with varying metatarsal dimensions, and one person who is affected possesses the pattern of clinodactyly. Non-sense variants and frameshift variants occur in the *KIAA0825* gene which leads to the cause of PAPA10 (Ullah *et al.*, 2019).

xi. Postaxial Polydactyly type A 11 (PAPA11)

A non-syndromic recessive disorder called PAPA11 has symptoms like PAP in the upper as well as lower limbs along with syndactyly in the middle toes (Ahmad *et al.*, 2023). Recent research has connected PAPA11 in a single Pakistani family to a biallelic missense variation in the Dachshund homolog 1 gene (*DACHI*) on 13q21.33 chromosome [c.563G>A; p.(Cys188Tyr)] with normal parents with no skeletal abnormalities (Umair *et al.*, 2021).

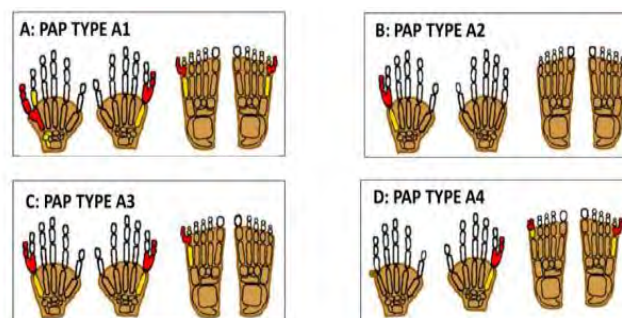


Figure 1.9: (a): (Ahmad *et al.*, 2023) **(A):** Triphalangeal thumbs, syndactyly wide, and PAP make up the majority of PAPA1, **(B):** PAPA2 displays unilateral PAP that is isolated, **(C):** The bilateral digits of PAPA3 are functional and well-developed, **(D):** Partial cutaneous polydactyly and PAP are two traits that distinguish PAPA4

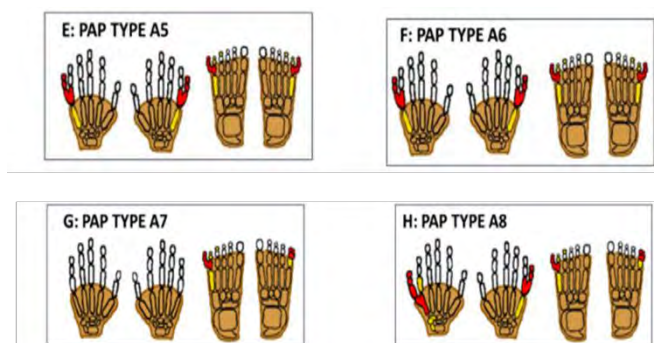


Figure 1.9: (b): (E): PAPA5 denotes the bilateral postaxial polydactyly, **(F):** PAPA6 displays fifth finger duplication either unilateral or bilateral with a duplicated distal phalanx of the 5th finger, where the red color in the figure depicts the affected digits in specific PAPA, **(G):** PAPA7 contains PAP limited to lower limbs, well-developed nails, and Brachydactyly in some cases, **(H):** PAPA8 represents PAP but no duplications of digits

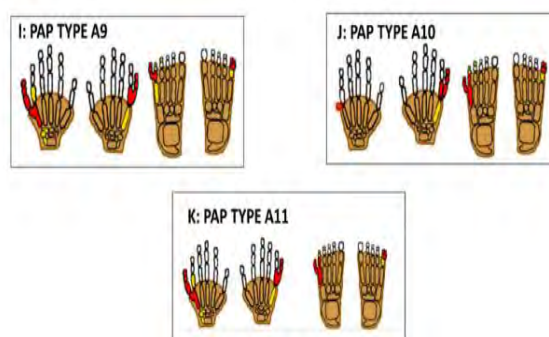


Figure 1.9: (c): (I), (J), and (K): PAPA9, 10, 11 comprise PAP in limbs but type A PAP, clinodactyly in PAPA10, and mild syndactyly are also observed in PAPA11, respectively.

Table 1.2: PAP Classification

Phenotype	OMIM ID	Locus	Genes	Inheritance
PAP1	174200	7p14.1	<i>GLI3</i>	AD
PAP2	602085	13q21-q32	<i>U</i>	AD
PAP3	607324	19p13.1-p13.2	<i>U</i>	AD
PAP4	608562	7q22	<i>U</i>	AD
PAP5	263450	13q13.3-q21	<i>U</i>	AR
PAP6	615226	4p16.3	<i>ZNF141</i>	AR
PAP7	617642	7p22.3	<i>IQCE</i>	AR

PAP8	618123	12q13.3	<i>GLI1</i>	AR
PAP9	618219	8q22.1	<i>FAM92A</i>	AR
PAP10	618498	5q15	<i>KIAA0825</i>	AR
PAP11	603803	13q21.33	<i>DACHI</i>	AR

U: unknown, AD: autosomal dominant, AR: autosomal recessive

2. Postaxial Polydactyly type B (PAPB)

This form of polydactyly is more prevalent. On the left side of the hand or foot, there is a vestigial ulnar (or fibular) finger that is ineffective, imperfectly developed, and without bone connections. The ulnar side of the fifth finger ranges in size from a tiny protuberance to a spine-like extension. The ulnar side of the fifth finger ranges in size from a tiny protuberance to a spine-like extension. It is connected by a small neurovascular stem (Castilla *et al.*, 1973). The most affected areas include the left hand and upper limbs. Since the inherited characteristics of this kind of polydactyly are more complex, the predicted penetration is around 43% (Castilla *et al.*, 1973; Holmes *et al.*, 2018). Variations in *GLI3* localized at chromosome 7p14.1 result in PAPB (Furniss *et al.*, 2007; Ullah *et al.*, 2018).

PAP categories A and B have historically been two distinct and biologically diverse communities due to their varied segregation patterns and independent frequencies (Castilla *et al.*, 1973; Temtamy and McKusick, 1978).

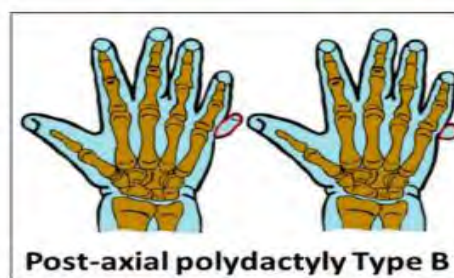


Figure 1.10: Diagram show postaxial polydactyly type B (PAPB) (Ahmad *et al.*, 2023)

III. Complex Polydactyly

These polydactylies fall under this classification since they do not meet the well-known pre-axial or post-axial phenotypes. The complex polydactyly is categorized into separate following types (Malik, 2014).

i. Mesoaxial or Central Polydactyly

One of the additional rings, index, or middle fingers on the hand or foot is duplicated in central polydactyly, a very uncommon phenotype. The ring finger is rarely suffering, while the index finger is more frequently impacted. It accounts for 5% to 15% of all polydactylies, which is significantly less prevalent than postaxial or preaxial polydactylies. It contains an autosomal dominant pattern (Graham and Ress, 1998). The second toe is usually duplicated, while foot central polydactyly is quite uncommon (Ishigaki *et al.*, 2021). Mesoaxial polydactyly, Holzgreve syndrome, and central polydactyly are all connected to split-foot deformity. The only known gene linked to central polydactyly is *CPLANE1* (Kyriazis *et al.*, 2023).

Based on the features of the duplicated finger, three types of central polydactyly are recognized. Type I, the duplicated finger does not have any ligamentous connections. Type II, Duplications share a joint such as the bifid metacarpal, or phalanx with the next finger and have osseous (normal) and soft-tissue structures within the duplicated digit. There are 2 sub-classes of Type II. Type IIa, there is no simultaneous syndactyly. Type Iib, the occurrence of concurrent syndactyly. Duplicate ray of Type III with a completely developed metacarpal (Bubshait, 2022).

ii. Mirror-Image Polydactyly (MIP)

Mirror-image hand or foot polydactyly is the presenting feature of this uncommon non-syndromic limb defect. The deformity might be unidirectional, bidirectional, or very infrequently tetramelic. The congenital anomaly may appear alone or in combination with other congenital abnormalities. Segregation pattern of MIP is autosomal dominant (Malik, 2014). *PITX1* and *MIPOLI* genetic variations have been recently identified in MIP. It is also caused by a unique high-mobility group box-1 *HMGB1* gene variation (Elsner *et al.*, 2021; Kyriazis *et al.*, 2023).

iii. Palmer and Dorsal Polydactyly

Palmer polydactyly is a highly uncommon condition in which an additional finger commonly grows from the ventrum or dorsum of the autopod. It could seem like a tiny skin, a finger with or without a nail that has been transplanted as an attachment into the autopod, or as a digit that is only partially grown (Umair *et al.*, 2018).

iv. Haas Type Polysyndactyly

Complete cutaneous syndactyly of all hand fingers and, sometimes, suffering foot toes are the hallmarks of Haas-type polysyndactyly. Polydactyly with six digits and six metacarpals is a common presenting feature. It is passed down through the autosomal dominant gene (Kyriazis *et al.*, 2023). Haas-type polysyndactyly was identified to have variations in the *LMBR1* gene's ZRS domain and other ZRS point mutations as well (Wieczorek *et al.*, 2010; Lohan *et al.*, 2014).

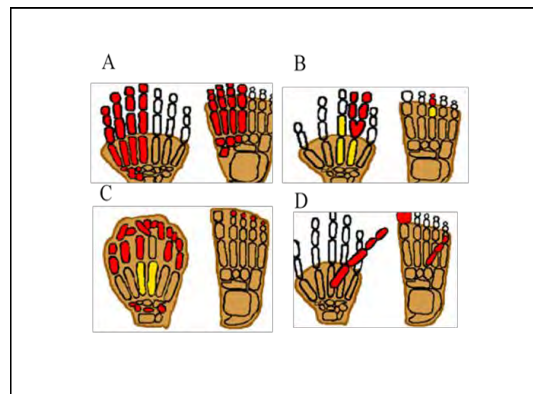


Figure 1.11: shows types of complex polydactyly (A): Mirror image polydactyly (B): Central or mesoaxial polydactyly in hands and foot (C): Haas type polydactyly and it contains complete syndactyly (D): Palmer and dorsal polydactyly contain a digit with partially grown (Umair *et al.*, 2018)

Aims and Objectives

Conclusively, herein two families were recruited from the Pakistani population to identify the genetic causes leading to hereditary skeletal disorders. The aim of the current study was to identify genetic variants in both families exhibiting polydactyly phenotype. For this purpose, the extracted DNA from the families was screened for variant identification. Whole Exome Sequencing (WES) was conducted on Family A, and potential variants in four genes, including *BPTF*, *TLX2*, *KIAA0513*, and *DYNC2H1* were identified through diverse bioinformatic tools. Subsequently, confirmation of their

segregation within the family was accomplished via conventional Sanger DNA Sequencing. Polymorphic microsatellite markers, linked to candidate genes (*GLI1*, *GLI3*, *EVC*, *EVC2*, *DYNC2H1*, *MIPOL1*, *IQCE*, *FAM92A1*) were genotyped in family B. This family failed to show a linkage with the reported gene of EVC syndrome. Therefore, WES is recommended for family B for the identification of other novel genes.

MATERIALS and METHODS

Study Subjects and Ethical Approval

The research presented in this thesis examined both the clinical and genetic characterization of two families underlying skeletal deformities. The Institutional Review Board (IRB) of QAU, Islamabad, granted ethical permission for the research's conduction. To collect blood samples, families were visited in their hometowns. Additionally, consent for the publication of photographs, and clinical and genetic data of affected participants were obtained with their permission.

Pedigree Construction

The families were interviewed about their extensive history and clinical data during the visit. According to the pedigree design (Bennett *et al.* 1995), a single horizontal line represented the marriage while double lines represented consanguineous unions, and vertical lines were used for the identification of generations. On the other hand, colorless squares and circles denoted healthy males and females, respectively, while darkened ones were used for affected members. The departed family members were represented as squares and circles crossed by an inclination. Roman numbers from top to bottom denoted each succeeding generation and Arabic numerals were used for each generation member.

Blood Sample Collection

Using sterilized syringes, specifically, those measuring 10ml (BD 0.8mm x 38mm 21G x $1\frac{1}{2}$ TW, Franklin Lakes, USA), blood samples were taken from both the unaffected and affected family members. The blood samples were immediately transferred to a vacutainer containing EDTA (ethylene diamine tetraacetate) to prevent blood clots. Before extracting the DNA, the acquired blood samples were stored at 4⁰C.

Genomic DNA Extraction

Both the commercially available kits and manual phenol-chloroform procedures were applied to isolate genomic DNA from the blood samples of healthy as well as affected family members.

Extraction of Genomic DNA by Phenol-Chloroform Method

Extraction through the phenol-chloroform method requires two days.

Day 1st

The initial stage consisted of obtaining 700µl of blood, adding an equal volume of Sol A, and gently vortexing the tube four to six times to mix the components in a 1.5ml eppendorf tube. After mixing, the eppendorf tube was kept at room temperature for approximately an hour. Centrifuge the eppendorf tube for 1 minute at 13,000 rpm after incubation (eppendorf Microfuge, 5415D, USA). The nuclear pellet was re-suspended in 500µl of Sol A in the third stage, following the removal of the supernatant. After dissolving in Sol A, the pellet was centrifuged once more for 1 minute at 15,000 rpm. Remove the supernatant and resuspend the nuclear pellet in 400µl of Sol B. In the last step of day one, we added 10µl of proteinase K and 17µl of SDS (20%) to the eppendorf tube that contains the pellet. After dissolving the pellet, the mixture was incubated at 37°C for an overnight period.

Day 2nd

On the next day, an equal volume of solution C and solution D (each 250µl) was added to the tube containing dissolved pellets and centrifuged for 10 min at 13,000 rpm. Two different layers were formed after centrifugation. DNA-containing material from the top layer was pipette-picked and transferred to fresh eppendorf tubes. After adding 500µl of Sol-D, the eppendorf tubes containing the DNA undergo another 10-minute centrifugation at 13,000 rpm. The outermost layer was once more taken out with a pipette and put in new eppendorf tubes. After adding 500µl of chilled isopropanol and 55µl of 3M sodium acetate (pH 6), the DNA-containing eppendorf tubes were gently twisted multiple times to produce precipitation of the DNA. The eppendorf tubes were centrifuged once more for 10 minutes at 13,000 rpm to precipitate the DNA into a pellet. The supernatant was once again removed before the particle was washed with 200µl of chilled 70% ethanol. Using concentrator 5301 (Eppendorf, Hamburg, Germany), the DNA was dried for 7 to 12 min at 45°C after the ethanol had been carefully discarded. Finally, the DNA was dissolved in 150µl of Tris-EDTA (TE) buffer after being incubated for an overnight duration at 37°C in an incubator. At 4°C, stock DNA was

preserved. Solutions and their compositions in the phenol-chloroform method are mentioned in **Table 2.1**.

Table 2.1: Solutions and their compositions used in the phenol-chloroform method

Solutions	Composition
Solution-A	Sucrose [0.32M] + MgCl ₂ [5mM] + Tris [10mM: 7.5pH] + 1% (v/v) TritonX-100
Solution-B	EDTA [2mM: 8.8pH] + NaCl [400mM] + Tris [10mM: 7.5pH]
Solution-C	Phenol
Solution-D	Chloroform + Isoamyl-alcohol [24:1]
70% Ethanol	Absolute Ethanol [70ml] + Distilled water [30ml]
20% SDS	10g SDS in 50ml distilled water

Extraction of Genomic DNA by Kit Method

A commercial reagent or kit from Sigma-Aldrich called the Gene-Elute Blood Genomic DNA extraction kit was used to extract genomic DNA. The steps involved in this are the following.

- About 200µl whole blood sample, 200µl of lysis buffer, and 20µl of PK enzyme were mixed in a 1.5ml tube.
- The mixture was placed in a water bath and incubated for 10 minutes at 55°C.
- After adding 200µl of cold, 100% ethanol to the mixture, it was vortexed for about 15 seconds. The mixture was given a quick spin at 3,000rpm, and then moved to the miniprep column (Sigma-Aldrich USA).
- Following 1 minute of 8,000rpm centrifugation, the columns were shifted to different tubes.
- Then the washing process was repeated twice, every time centrifuging at 13,000rpm after adding 500µl washing buffer. An elution buffer (240µl) was added in the center of the columns after an empty spin, to

thoroughly rinse the columns. After that, the sample was incubated at 25°C for 10 minutes.

- Then, using a high-speed centrifuge, DNA was extracted from the columns and placed in tubes.

Agarose Gel Electrophoresis (1%)

To check the integrity and quality of DNA, Agarose Gel Electrophoresis was performed. For DNA visualization, 1% agarose gel was prepared. The composition of the gel is mentioned in **Table 2.2**. A cylindrical container containing 45 ml of distilled water was filled with 5 ml of 10X TBE Borate-EDTA (TBE) buffer to make a total volume of 50ml. Added the solution to a beaker holding 0.5g of agarose powder. The turbidity agarose solution was now microwaved for 1-2 minutes to create a transparent solution and ensure that the agarose was fully dissolved. After that, 3 to 4µl of ethidium bromide (Et. Br) was added and mixed as an intercalating agent. Afterward, the gel mixture was poured in the gel casting tray which was already loaded with the combs for pore generation. The gel was allowed for solidification for 20 to 30 minutes at room temperature. The gel was then hardened and transferred into an electrophoresis tank containing 1X flowing buffer. For sample loading, the DNA sample and loading dye (Bromophenol blue) with a 1:1 ratio were mixed and loaded in the wells of the gel. The apparatus was connected to the power supply and ran on 80V for 20-30 minutes. U.V. Trans-illuminator (Biometra, Gottingen, Germany) was used to visualize the DNA bands.

Table 2.2: Description of solutions composition used in agarose gel electrophoresis

Chemicals	Compositions
Agarose	0.5g
Ethidium Bromide	4µg/ml
TBE (10X) buffer	EDTA [0.032M: 8.3pH] + Boric ac id [0.025M] + Tris [0.89M]
Gel Loading Dye	Bromophenol blue dye [0.25%] + Sucrose [40%]

DNA Quantification and Dilution

Measurements were acquired at an optical density (OD) of 260 nm using the Colibri micro-volume spectrophotometer (Titertek Berthold, Germany) for the quantitative measurement of DNA. The DNA concentrations were calculated in ng/ μ l units after a 2 μ l of TE buffer was used as a blank and a 2 μ l of DNA sample was inserted into the spectrophotometer. The addition of PCR water diluted the DNA to 20–30 ng/ μ l.

Genotyping

Microsatellite markers were used to search for homozygous regions underlying skeletal disorder in family A for the known loci and genes. The genetic distance between the microsatellite markers that surrounded these known loci, which were located using the UCSC genome browser. Five to ten microsatellite markers within centimorgans (cM) of the specific locus and gene were employed to confirm the homo and heterozygosity of these markers in affected and normal individuals.

Polymerase Chain Reaction (PCR)

The DNA dilutions have proceeded for amplification through polymerase chain reaction using specific STS markers. For the preparation of the PCR reaction mixture, 200 μ l PCR tubes were used (Axygen, California, USA). The PCR test was performed using a T3 Thermocycler (Biometra, Germany). The components and concentrations of chemicals used in PCR are discussed in **Table 2.3**. Following the loading of the PCR tube onto the thermocycler, amplification was carried out under the mentioned parameters in **Table 2.4**. The results of PCR amplification were afterward visualized and confirmed on 2% agarose gel.

Table 2.3: PCR Components and its concentrations

Components	Concentrations
Template DNA	2 μ l
PCR Buffer	2.5 μ l
MgCl ₂	2 μ l
dNTPs	0.5 μ l
Taq polymerase	0.5 μ l

Forward primer	0.5 μ l
Reverse primer	0.5 μ l
PCR Water	16.5 μ l
Total volume	25 μ l

Table 2.4: Thermocycler conditions used for the amplification of the PCR product

Steps	Sub-steps	Temperature	Time
Initial denaturation		96°C	05 minutes
35 cycles	a. Denaturation	96°C	35 seconds
	b. Annealing	57-64°C	35 seconds
	c. Extension	72°C	35 seconds
Final Extension		72°C	05 minutes

Polyacrylamide Gel electrophoresis (Vertical Gel)

The PCR-amplified product was resolved on 8% non-denaturing polyacrylamide gel electrophoresis (PAGE) after amplification. A 50ml solution needed to be created by the instructions in Table 2.2 to prepare one polyacrylamide gel. Between plates that were 1.5 mm apart, the gel solution was poured, and a comb was added. For around 35 to 40 minutes, at room temperature, let the gel set and polymerize. Before loading the samples, the amplified product and bromophenol blue (6 μ l) were thoroughly mixed. The gel was operated in a vertical tank at 147–155 volts for roughly three hours. With the use of an Et. Br solution staining gel and a UV transilluminator (Biometra, Gottingen, Germany), the electrophoresis procedure was carried out using 1X TBE buffer as the running buffer. DC 290 camera system (Kodak, Digital Sciences, New York, USA) was used to take the pictures.

Table 2.5: Composition and Quantities of Solutions Used for the PAGE Preparation

components	Composition	Quantities
Solution of 30% acrylamide	A) Acrylamide (29g) B) N, N' Methylene bisacrylamide (1g)	13.5ml
10-X TBE	A) Tris 0.89M B) Borate 0.025M C) EDTA 0.02M	5ml
10% APS	A) 5g of Ammonium Sulphate B) 45ml of distilled H ₂ O	400µl
TEMED	N, N, N,' N'-Tetra methyl ethylene diamine (Sigma Aldrich, USA)	35µl
Distilled H ₂ O	-	Raised Volume to 50ml

Whole Exome Sequencing (WES)

WES was conducted at the Yale Centre for Genome Analysis (YCGA), which was subsidized by the Higher Education Commission (HEC) of Pakistan, the Yale Pediatric Genome Discovery Programme (PGDP), the Yale School of Medicine in Connecticut, USA, and the Center of Inherited Diseases at Taibah University Madinah, SA. Sample DNA (3-5µg) of whole members of the first family and a single member of the second family was provided for WES to YCGA. IDT-xGen Capture kit from the USA was used to prepare the sequencing library, and the Illumina (HiSeq4000) platform carried out the WES. Paired-end sequence readings were transferred to FASTQ format and compared to the UCSC reference human genome (hg19). The Genome Analysis Tool kit (GATK.v3.4) was used for Variants (CNV, SNV) detection, variant calling, indel realignment, removal of duplications, and Quality recalibrations (Van-der-Auwera *et al.*, 2013) and AnnoVar was used for Annotation. A mean depth of 80-120 independent

reads per targeted base was used to sequence the members. On average, 93.7-94.8% of all the samples had more than eight independent reads, indicating high confidence in all the exome variants. Variants with depth score ($QD \geq 2$) and high-quality sequencing reads with at least 10 total reads were filtered. Variants were then selected based on their nature (frame-shift mutant, splice-site variant, missense variant), function, and expression. The following criteria were set for shortlisting candidate genes with Allele frequency 13, and the nature of the inheritance pattern (autosomal dominant or recessive).

Variants were chosen after analyzing them on various databases:

- gnomAD (<https://gnomad.broadinstitute.org/>)
- MutationTaster (<https://www.mutationtaster.org/>)
- VarSome (<https://varsome.com/>)
- ClinVar (<https://www.ncbi.nlm.nih.gov/clinvar/>)
- HGMD (<https://www.hgmd.cf.ac.uk/>)
- DynaMutt (<https://biosig.lab.uq.edu.au/dynamut2>)

Sanger Sequencing confirmed further segregation of the variants in all family members.

Primer Designing

Exon-specific primers were created using software that was easily accessible online. Primer3 is one of the promising programs for designing primers (<https://primer3.ut.ee/>). Primer Stat software (https://www.bioinformatics.org/sms2/pcr_primer_stats.html) was used to assess and confirm additional primer parameters. The GC content, self-annealing, annealing temperature [T_m], and primer dimer formation were all improved during primer design in primer stat. The BLAST-like alignment program (BLAT) (<https://genome.ucsc.edu/cgi-bin/hgBlat>) was used to choose the primers that produced a single hit.

Pre-sequencing PCR

Exons of targeted/specific genes were amplified using pre-sequencing PCR. The 25 μ l reaction mixture was made up of 1.5 μ l of DNA, 0.7 μ l of forward and reverse primers,

2 μ l of MgCl₂, 2.5 μ l of PCR buffer, 0.5 μ l of dNTPs, 0.5 μ l of Taq polymerase, and 17.5 μ l of PCR water. Under the circumstances described above, the PCR was completed using the thermocycler, and the results were examined on a 2% agarose gel.

Agarose Gel (2%)

The PCR-amplified product was examined on a 2% agarose gel after being sequenced. The following ingredients were combined in a beaker: 10ml 10X TBE buffer, and 90ml distilled water. After that, 2g of agarose was added and the mixture was microwave-heated for 2 minutes. Et. Br (6 μ l) was added and thoroughly mixed into the solution after heating. The combs were then positioned to form the wells after the gel had been poured into a gel tank. To completely solidify, the gel was left at room temperature for 30–40 minutes. After setting, the gel was inserted into a gel tank with a 1X TBE running buffer. Before loading into the gel, 3 μ l of each sample of DNA and 3 μ l of bromophenol blue were combined. The bands were then visible in the gel doc after the electrophoresis procedure was completed at 95V for 40 minutes.

Purification of Amplified PCR Product

Following the amplification of the targeted PCR product, it was purified using Invitrogen's Axygen Biosciences PCR Clean-up Kit by following the methods listed below.

- The amplified product was added to 75 μ l of binding buffer and thoroughly mixed. Put the mixture into a column with a 2 ml collecting tube. Centrifuge it for 1 minute at 13,000 rpm. A collecting tube was used to collect the filtrate, which was then taken out.
- The column was double-washed using 400 μ l and then 350 μ l of washing buffer, each time spinning for one minute at a speed of roughly 13,000 rpm. Liquid from a centrifuge is drained from the collecting tube.
- The purification column performed a 2-minute empty spin after being discarded to remove contaminants and impurities.
- After being discarded, the purification column performed a 2-minute empty spin to remove contaminants and impurities.
- After 5 minutes of incubation at room temperature, the column was then transferred to an eppendorf tube, and 22 μ l of elution buffer was added.

- It was then centrifuged for 10 minutes at a resolution speed of 13,000 rpm with the purification column and eppendorf tube attached. To examine the purified DNA product on a 2% agarose gel electrophoresis, 3 μ l of product and 1 μ l of bromophenol blue were mixed and kept at 4 °C.

Sanger Sequencing Analysis

Purified base pair products of certain sizes were subjected to commercial sanger-sequencing, and the results were examined using the BioEdit alignment program (<http://www.mbio.ncsu.edu/bioedit.html>). Using reference genes from the UCSC genome browser, chromatograms of affected and unaffected people were obtained.

Table 2.6: Primer sequences of the genes involved in Polydactyly

Genes	Primer Sequence [5'→3']	Base Pairs	Product size
<i>BPTF-F</i>	AAACAAGATGGCGGCTGAAG	20bp	699bp
<i>BPTF-R</i>	CATCTCATCCTCCTCGTCGT	20bp	
<i>KIAA0513-F</i>	GGAATAGCACCGTTACTGGC	20bp	337bp
<i>KIAA0513-R</i>	GGACAAAGGCAGCTAGAAGTG	21bp	
<i>TLX2-F</i>	GCACAGGTCAAACGTGGT		337bp
<i>TLX2-R</i>	CGGACACTGAAGCCACTTTG		
<i>DYNC2H1-F</i> A	GCTCCTCTCTCCCTTCACT	20bp	598bp
<i>DYNC2H1-R</i> A	CACTACACTCCATCCAGCCT	20bp	

<i>DYNC2H1-F</i> <i>B</i>	AGACAGGGACGATTACAATTCA	22bp	561bp
<i>DYNC2H1-R</i> <i>B</i>	ACATTGTGCACATGTACCCTAAA	23bp	

Table 2.7: List of Microsatellite Markers Used for Homozygosity Mapping

S. No.	Targeted Gene	Locus	Markers	Centi-Morgan
i.	<i>GLII</i>	12q13.3	D12S1298	74.31
			D12S305	74.31
			D12S90	73.71
			D12S1691	73.71
			D12S1632	72.58
			D12S1707	70.8
			D12S1724	70.52
ii.	<i>GLI3</i>	7p14.1	D7S2548	62.57
			D7S671	62.77
			D7S691	62.99
			D7S2428	64.26
			D7S2436	66.25
iii.	<i>IQCE</i>	7p22.3	D7S2474	1.94
			D7S1532	3.12
			D7S616	4.79
			D7S2484	5.35
			D7S2521	5.38
			D7S531	5.81
			D7S464	5.83

			D7S2424	5.83
iv.	<i>DYNC2H1</i>	11q22.3	D11S898 D11S1982 D11S1924 D11S1339 D11S4108 D11S1913 D11S4951 D11S1302 D11S2000	109.28 109.28 109.77 110.21 110.21 111.12 111.12 111.47 111.71
v.	<i>EVC1</i>	4p16.2	D4S2925 D4S2285 D4S431 D4S2366 D4S2935	7.17 7.97 12.41 12.57 13.21
vi.	<i>EVC2</i>	4p16.2	D4S2925 D4S2285 D4S431 D4S2366 D4S2935	7.17 7.97 12.41 12.57 13.21
vii.	<i>FAM92A1</i>	8q22.1	D8S1988 D8S270 D8S1699	103.15 102.97 105.57

viii.	<i>MIPOLI</i>	14q13.3	D14S599	34.48
			D14S1014	35.77
			D14S253	35.77
			D14S286	39.07
			D14S579	39.98
			D14S79	40.37
			D14S301	40.84

RESULTS

Families Description

Two families (A and B) from different regions of Pakistan were recruited for the present study. Family A manifested characteristic phenotypes of pre and post-axial polydactyly while family B exhibited EVC syndrome clinically characterized by short stature, polydactyly, nail and teeth anomalies.

Family A

Family A labeled as Lab ID BD-344, which showed the features of Polydactyly, was sampled from Lakki Marwat District in Khyber Pakhtunkhwa province of Pakistan and a pedigree of two generations was constructed based on the information provided by elders of the family (**Figure 3.1**). Pedigree manifested autosomal recessive inheritance pattern with consanguineous marriage.

Clinical Features

Family was represented with four participants (I-1, II-1, II-3, II-4) with two affected member (II-3, II-4) showing polydactyly. Such as the affected individual (II-3) manifested preaxial polydactyly in the right hand and the affected individual (II-4) manifested postaxial polydactyly in the left hand as shown in **Figure 3.2**. Both of the members did not exhibit any other abnormality.

Genetic Investigations

Blood samples of two affected sons (II-3, II-4) along with the normal father (I-2) and a son (II-2) were collected for genetic assessment. The DNA of the affected members (II-3 and II-4) was subjected to Whole Exome Sequencing. A total of 36,535 variants were filtered through exome sequencing analysis. To find disease-causing variants, various filters were applied. The focus was to only search for pathogenic missense, non-synonymous, frame-shift, and non-sense deletions/insertions. The non-coding, intronic, intragenic, and low-quality variants were excluded. The variants were selected by using the following criteria: allele frequency ≤ 0.005 , CADD Phred score of ≥ 13 , and splice site (+/- 12bp). Four variants of different genes were shortlisted for segregation analysis. This included a missense variant [c.847G>A, p.(Glu283Lys)] in exon 8 in the *KIAA0513* gene, a missense variant [c.206G>T, p.(Gly69Val)] in exon 1 in *BPTF* gene,

a missense variant [c.665C>T, p.(Ala222Val)] in exon3 in *TLX2* gene, and compound heterozygous variant with an intronic variant [c.195+12T>A] and a missense variant [c.2527G>A, p.(Ala843Thr)] in in exon 17 *DYNC2H1* gene. **Table 3.1** shows the above-mentioned genes selected for further investigations through segregation analysis. However, due to a lack of available time for degree completion, segregation analysis was performed only in two genes, including *BPTF* and *KIAA0513*. In both these cases, the variants failed to segregate with the phenotypes within the family.

Family B

Family B, labeled as Lab ID BD-829, showed the features of Ellis-Van Creveld syndrome. Sampled from D.G. Khan City in the Punjab province of Pakistan. The pedigree of three generations was constructed based on the information provided by the elders of the family (**Figure 3.3**). Pedigree exhibited an autosomal recessive inheritance pattern with consanguineous marriage. Pedigree was composed of 14 individuals including one affected individual in the 2nd generation and two affected individuals in the 3rd generation of the family.

Clinical Features

Affected individuals were found to have Ellis-Van Creveld syndrome. These individuals show clinical features of short stature, post-axial polydactyly, conical teeth, and leukonychia nails. One affected member (II-2) of 2nd generation manifested the features of post-axial polydactyly in the right foot and bilateral in the hands. One affected member (III-3) of 3rd generation manifested the features of bilateral post-axial polydactyly in hands.

Genotyping and Linkage Analysis in Family B

Blood samples of two affected individuals (II-2 & III-1) along with the normal father (I-1), mother (I-2), and son (II-1) were taken for genetic assessment. Family B was tested, using polymorphic microsatellite markers, for linkage to the genes that were previously reported to cause Ellis-Van Creveld syndrome. Highly polymorphic microsatellite markers present in close vicinity of the causative genes were selected (**Table 3.1**). The tested candidate genes included *GLII* (12q13.3), *GLI3* (7p14.1), *DYNC2H1* (11q22.3), *IQCE* (7p22.3), *EVC1* (4p16.2), *EVC2* (4p16.2), *FAM92A* (8q22.1), *MIPOLI* (14q13.3). Genotyping of the markers present in the vicinity of

genes *GLI1* and *GLI3* (Figure 3.5), *IQCE* and *DYNC2H1* (Figure 3.6), *EVC* and *EVC2* (Figure 3.7), *FAM92A1* and *MIPOL1* (Figure 3.8) failed to show any homozygous pattern for alleles, indicating that the family was not linked to any of the selected genes.

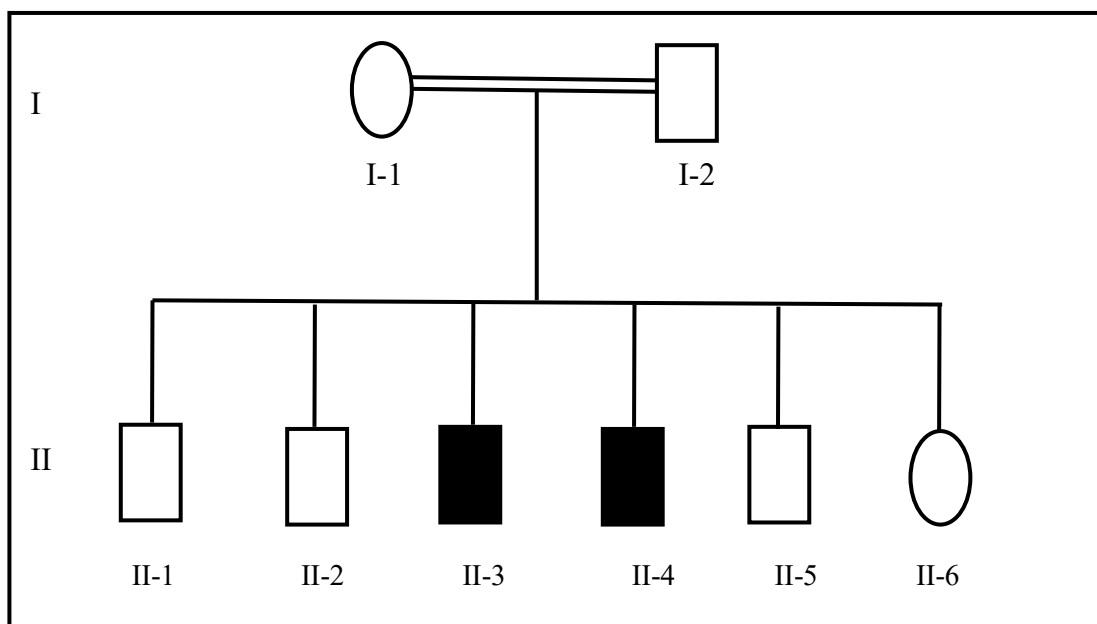


Figure 3.1: The pedigree of two generations in family A exhibiting an autosomal recessive pattern of inheritance in pre-axial and post-axial polydactyly. Filled and non-filled circles, respectively, indicate affected and normal females. Similarly, both the affected and normal males are shown by squares either filled or non-filled. The consanguineous marriages are denoted by two horizontal lines in this diagram. While Roman numerals are utilized for determining the generations and Arabic numerals are used for the identification of the number of members in the family. The symbol of Asterisk (*) was intended for those members of the family whose blood samples were taken.



Figure 3.2: Clinical characteristics observed in the affected sons (II-3 and II-4) of family A. The features of affected patients are the following. **(A):** Affected son (II-3) shows pre-axial polydactyly, the first metacarpal being excessively thin and lengthy, and the thumb possesses an additional intermediate bone. **(B):** Another affected son (II-4) shows a small protrusion at the ulnar side of the fifth finger. **(C):** X-ray of the patient (II-3).

Table 3.1: Analysis of variants detected in exome data in family A

Family ID	A			
Gene	KIAA0513	BPTF	TLX2	DYNC2H1
Hg38 Position	16:85112554	17:65822046	2:74743126	11:102980510 11:103006630
Nature of Mutation	Missense mutation	Missense mutation	Missense mutation	Intronic splice site mutation, Missense mutation
Transcript	NM_014732 c.847G>A	NM_004459 c.206G>T	NM_016170 c.665C>T	c.195+12T>A NM_001080463 c.2527G>A
Protein	p.Glu283Lys	p.Gly69Val	p.Ala222Val	Intron p.Ala843Thr
No. of Homozygotes	0	0	0	1 1
Allele Frequency	0.00003579	0.000039	0.00002306	0.00005742 0.0004515
CADD Score	23.1	9.526	27.7	- 24.8
Mutation Taster	Disease-causing	Disease-causing	Disease-causing	Disease-causing
PolyPhen Score	Benign(0.001)	Possibly damaging(0.8)	Possibly damaging(0.613)	- Probably damaging(0.919)
SIFT	Tolerated(0.09)	Deleterious low confidence(0)	Deleterious(0)	- Tolerated(0.08)
Segregation	No	No	-	-

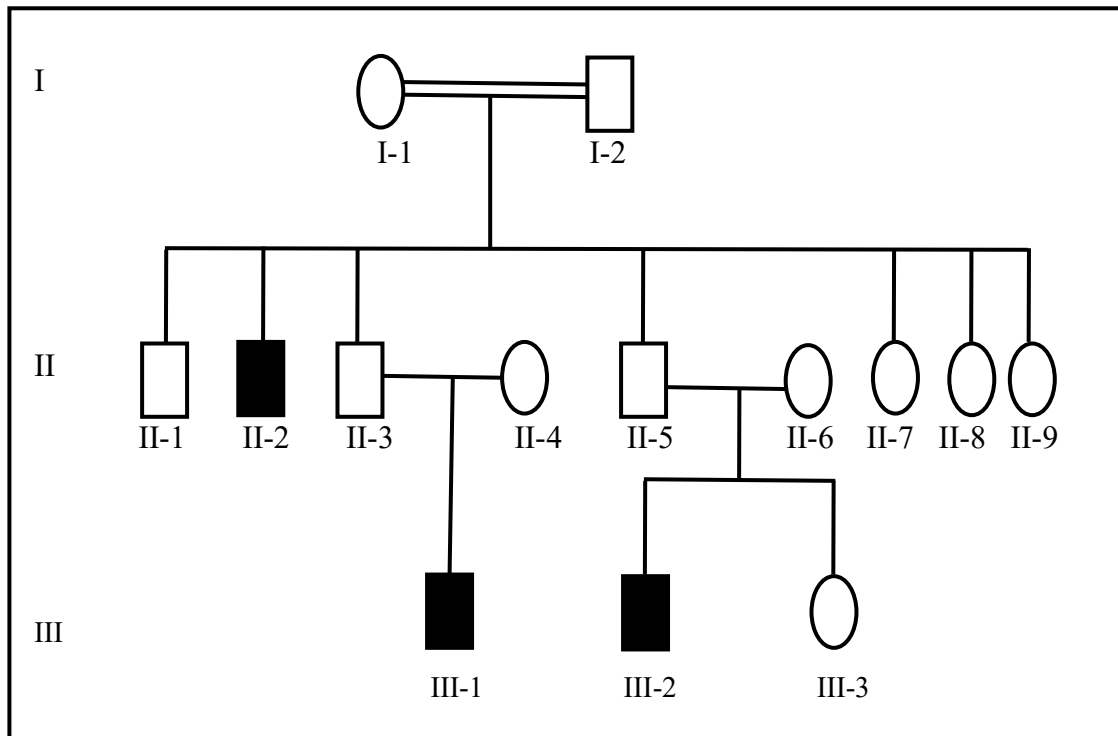
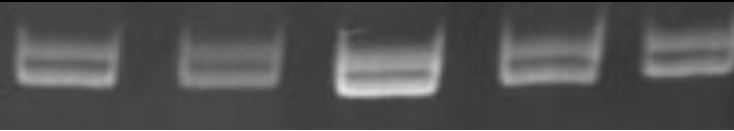
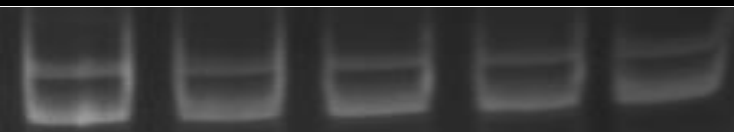
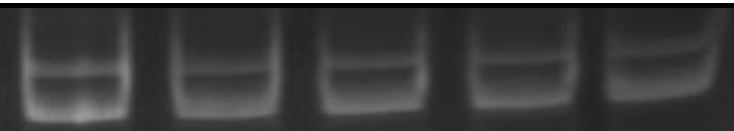
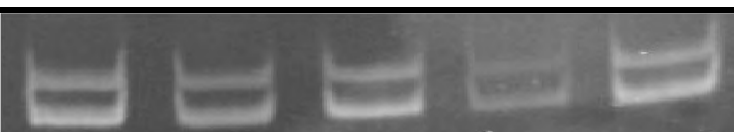




Figure 3.3: The pedigree of three generations in family B exhibiting an autosomal recessive pattern of inheritance in Ellis-Van Creveld syndrome. Filled and non-filled circles, respectively, indicate affected and normal females. Similarly, both the affected and normal males are shown by squares either filled or non-filled. The consanguineous marriages are denoted by two horizontal lines in this diagram. While Roman numerals are utilized for determining the generations and Arabic numerals are used for the identification of the number of members in the family. The symbol of Asterisk (*) was intended for those members of the family whose blood sample was taken.



Figure 3.4: Clinical features of Family B **(A):** Short stature **(B):** Conical teeth **(C):** leukonychia nails **(D):** Post-axial type A polydactyly in foot

Genotyping Results of Family B

<i>GLI1</i>									
S.No	Marker ID	Map Unit CM	N I-1	N I-2	N II-1	A II-2	A III-2		
i	D12S1298	74.31							
ii	D12S305	74.31							
iii	D12S90	73.71							
iv	D12S1691	73.71							
v	D12S1632	72.58							
<i>GLI3</i>									
S.No	Marker ID	Map Unit CM	N I-1	N I-2	N II-1	A II-2	A III-2		
i	D7S2548	62.57							

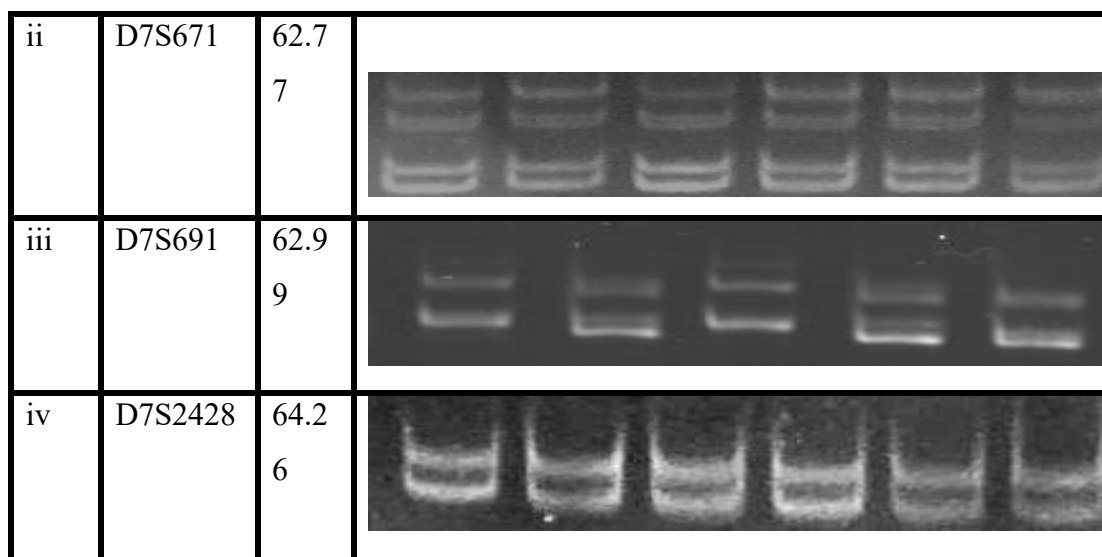
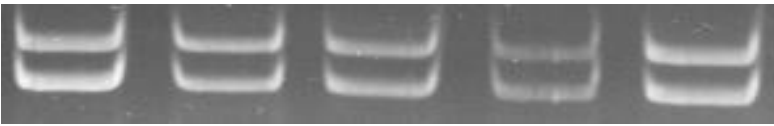
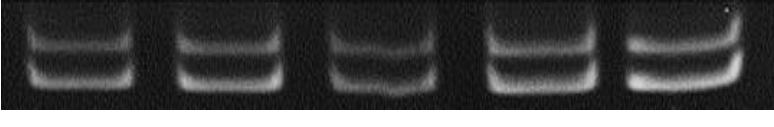
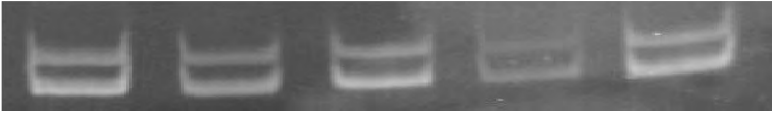


Figure 3.5: Polyacrylamide electropherogram, showing the pattern of alleles amplified with specific microsatellite markers flanking the *GLI1* and *GLI3* gene in family B. Roman numbers denote the generation numbers, and Arabic numbers denote the number of individuals in each generation of the family pedigree.

<i>IQCE</i>							
S. No	Marker ID	Map Unit CM	N I-1	N I-2	N II-1	A II-2	A III-2
i	D7S2474	1.94					
ii	D7S1532	3.12					
iii	D7S616	4.79					


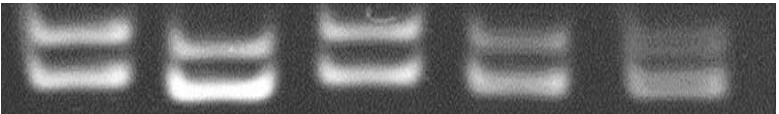

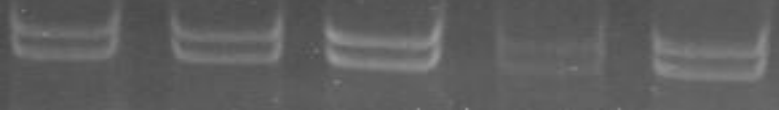
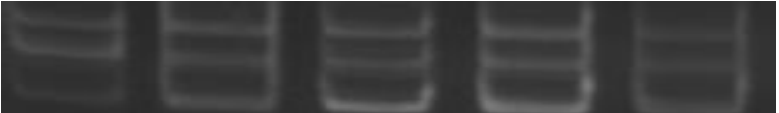


iv	D7S2484	5.35					
v	D7S2521	5.38					
<i>DYNC2H1</i>							
S. No	Marker ID	Map Unit CM	N I-1	N I-2	N II-1	A II-2	A III-2
i	D11S1924	109.77					
ii	D11S1339	110.21					
iii	D11S4108	110.21					
iv	D11S1913	111.12					
v	D11S4951	111.12					

Figure 3.6: Polyacrylamide electropherogram, showing the pattern of alleles amplified with specific microsatellite markers flanking the *IQCE* and *DYNC2H1* gene in family B. Roman

numbers denote the generation numbers, and Arabic numbers denote the number of individuals in each generation of the family pedigree.

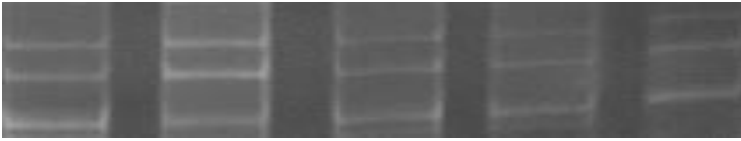
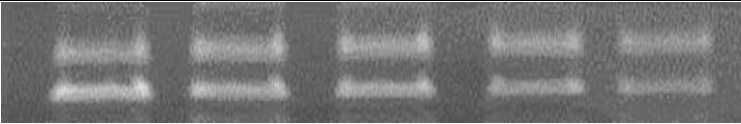

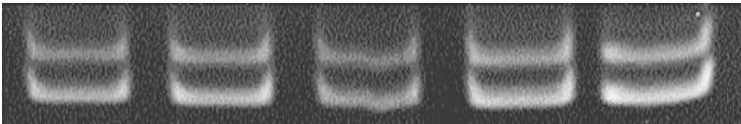
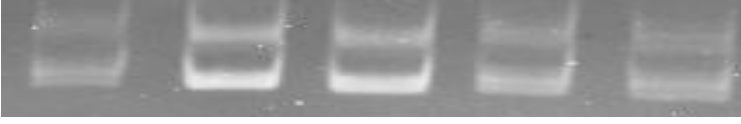

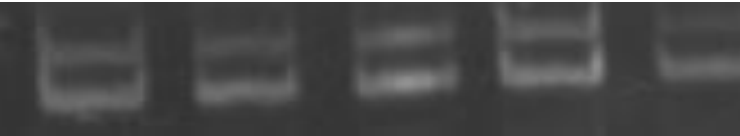



<i>EVC1</i> and <i>EVC2</i>								
S.No	Markers ID	Map Unit CM	N I-1	N I-2	N II-1	A II-2	A III-2	
i	D4S292 5	7.17						
ii	D4S228 5	7.97						
iii	D4S431	12.4 1						
iv	D4S236 6	12.5 7						
v	D4S293 5	13.2 1						

Figure 3.7: Polyacrylamide electropherogram, showing the pattern of alleles amplified with specific microsatellite markers flanking the *EVC1* and *EVC2* gene in family B. Roman numbers denote the generation numbers, and Arabic numbers denote the number of individuals in each generation of the family pedigree.

FAM92A1								
S.No	Marker ID	Map Unit CM	N I-1	N I-2	N II-1	A II-2	A III-2	
i	D8S1988	103.15						
ii	D8S270	102.97						
iii	D8S1699	105.57						
MIPOL1								
S.No	Marker ID	Map Unit CM	N I-1	N I-2	N II-1	A II-2	A III-2	
i	D14S599	34.48						
ii	D14S1014	35.77						


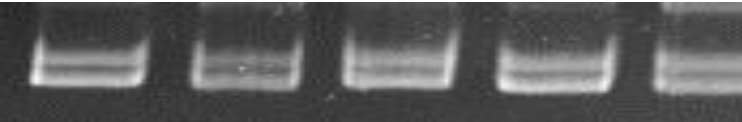

iii	D14S253	35.77	
iv	D14S286	39.07	
v	D14S579	39.98	

Figure 3.8: Polyacrylamide electropherogram, showing the pattern of alleles amplified with specific microsatellite markers flanking the *FAM92A1* and *MIPOL1* gene in family B. Roman numbers denote the generation numbers, and Arabic numbers denote the number of individuals in each generation of the family pedigree.

DISCUSSION

The skeletal system provides shape and support to the body, Protection of vital organs, Movement, Hematopoiesis, and Storage reservoir of minerals (salts, calcium, and phosphorus; (Krakow and Rimoin, 2010). Many genes or transcription factors and bone signaling pathways are involved in developing skeletons. Any mutation in these pathways or factors that disturbs the skeletal developmental process leads to Genetic Skeletal Dysplasia (GSD). Genetic mutations cause skeletal abnormalities. In the Pakistani population, several of these disorders segregating in autosomal dominant, recessive, and X-linked patterns have been characterized. GSD cases have been identified in all four provinces of Pakistan. GSDs and other uncommon genetic disorders receive very little attention in Pakistan. Consanguineous marriages are mainly the cause of genetic disorders and have appeared in many Pakistani provinces (Warman *et al.*, 2010; Mortier *et al.*, 2019; Umair *et al.*, 2019).

Polydactyly or polydactylism, is a genetic condition known as 'Hexadactyly'. Polydactyly is a type of skeletal abnormality characterized by extra digits on the radio-ulnar, tibiofibular, or both aspects of the limbs. Polydactyly can be inherited in syndromic and non-syndromic forms. In syndromic forms, polydactyly combines with multiple disorders such as Bardet Biedl syndrome (BBS), Poland syndrome, Greig syndrome, Carpenter syndrome, Ellis Van Creveld (EVC) syndrome, Pallister-Hall syndrome, and short rib polydactyly (Bubshait, 2022; Kyriazis *et al.*, 2023). Chondroectodermal dysplasia, which includes Ellis-Van Creveld Syndrome, is classified as ciliopathy and is caused by alteration at chromosome 4p16. EVC syndrome also has syndromic representation but in a recessive manner. Post-axial polydactyly, cardiac problems, dental and oral signs, leukonychia nails, and dwarfism are the characteristic features of EVC syndrome. Less frequent symptoms are post-axial polydactyly of feet, upper lips problem, and growth retardation (Thomas *et al.*, 2022; Da Silva *et al.*, 2023). On the other hand, based on the particular anatomical location of the duplicated digits, it can be divided into the following categories pre-axial, post-axial, complex polydactyly (Mirror image polydactyly, Haas polydactyly, Central polydactyly, Palmer polydactyly; Malik, 2014). Both the autosomal dominant and recessive patterns are typically seen and linked to a variety of genetic factors (Ahmad *et al.*, 2023).

In the current study, two Pakistani families with different phenotypes of non-syndromic polydactyly and EVC syndrome, having consanguineous marriages and segregating in an autosomal recessive form are described. These two families resided in remote areas of the country such as Punjab and KPK provinces. For this purpose, blood samples of both normal and affected members were collected for DNA extraction and further analysis. Family A consisted of two normal and two affected members. Clinical features of affected members are pre-axial and post-axial polydactyly with the consanguineous marriage, the two-generation pedigree predicted that the non-syndromic polydactyly would be inherited recessively. Two affected members proceeded to WES and the data was analyzed and variants in four genes (*KIAA0513*, *BPTF*, *TLX2*, *DYNC2H1*) were shortlisted for segregation analysis. All of these variants were first validated in terms of pathogenicity by several in-silico software including MutationTaster, SIFT, PolyPhen2, and gnomAD. Due to lack of time, segregation analysis of variants in two genes, *BPTF* and *KIAA0513*, were completed. In both cases, the variants failed to segregate with the phenotypes within the family. It is important and recommended that segregation analysis may be performed with variants found in the other two genes, *TLX2* (OMIM #604240) and *DYNC2H1* (OMIM #603297). The *TLX2* has expression in mouse limbs. For mouse mesoderm to mature, BMP signaling is necessary. So the target gene for BMP signaling is *TLX-2* (Tang *et al.*, 1998). *DYNC2H1* was selected for its expression in skeletal ciliopathies and it is involved in the transportation of ciliary protein. This process maintains the stabilization of primary cilia and it performs its function in hedgehog pathways which is important for skeletal development (Rohatgi *et al.*, 2007; Satir and Christensen, 2007; D'Angelo and Franco, 2009; Huber and Cormier-Daire, 2012). So according to the in-silico software, there is a possibility that the variants in these two genes may be responsible for causing phenotypes observed in family A.

Affected members in family B displayed the clinical features of EVC syndrome. The condition was found segregated in an autosomal recessive manner. All affected members in the family showed Post-axial polydactyly in hand and foot, leukonychia nails, and dwarfism. There was no additional abnormality in the affected members. Initially, linkage in the family was searched by genotyping genes-linked Polymorphic microsatellite markers. For this purpose, the DNA of five individuals, including two

affected and three healthy was genotyped with markers linked to *GLII* (12q13.3), *GLI3* (7p14.1), *DYNC2H1* (11q22.3), *IQCE* (7p22.3), *EVC1* (4p16.2), *EVC2* (4p16.2), *FAM92A1* (8q22.1), *MIPOL1* (14q13.3). Analysis of the results failed to show any homozygous pattern for alleles, showing no linkage to any of these selected genes. Therefore, it is suggested that a novel gene is involved in causing the disorder in the family. The DNA of an affected member in family B will be used for whole exome sequencing to find the causative variant and the gene.

In conclusion, this thesis aims to comprehensively examine the origins of skeletal disorders in two Pakistani families through the conduction of thorough investigations at both clinical and genetic levels. It involved detailed analysis and interpretation of clinical data for genetic identification and characterization of underlying phenotypes using WES and homozygosity mapping. Segregation analysis in family A was not completed owing to the limited time available for degree completion. As a consequence, it is strongly recommended to perform segregation analysis with variants found in the *TLX2* and *DYNC2H1* genes. Family B did not show linkage to the tested known genes underlying the phenotypes of EVC syndrome; therefore, it is presumed the involvement of novel genes in causing the phenotypes observed in the family.

REFERENCES

- Abbas S, Khan H, Alam Q, Mahmood A, Umair M (2023). Genetic advances in skeletal disorders: an overview. *J Biochem Clin Genet* 6; 57-57.
- Ahmad S, Ali MZ, Muzammal M, Mir FA, Khan MA (2022). The molecular genetics of the human appendicular skeleton. *Mol Genet Genom* 297; 1195–1214.
- Ahmad Z, Liaqat R, Palander O, Bilal M, Zeb S, Ahmad F, Jawad Khan M, Umair M (2023). Genetic overview of postaxial polydactyly: Updated classification. *Clin Genet* 103; 3-15.
- Ahmed H, Akbari H, Emami A, Akbari MR (2017). Genetic overview of syndactyly and polydactyly. *Plast Reconstr Surg*.
- Ali BR, Akawi NA, Chedid F, Bakir M, Ur Rehman M, Rahmani A, Al-Gazali L (2010). Molecular and clinical analysis of Ellis-van Creveld syndrome in the United Arab Emirates. *BMC Med Genet* 11; 1-7.
- Alman BA (2015). The role of hedgehog signalling in skeletal health and disease. *Nat Rev Rheumatol* 11; 552-560.
- Atasu ME (1976). Hereditary index finger polydactyly: phenotypic, radiological, dermatoglyphic, and genetic findings in a large family. *J Med Genet* 13; 469-476.
- Attanasio C, Nord AS, Zhu Y, Blow MJ, Li Z, Liberton DK, Morrison H, Plajzer-Frick I, Holt A, Hosseini R, Phouanavong S (2013). Fine tuning of craniofacial morphology by distant-acting enhancers. *Sci* 342; 1241006.
- Baldrige D, Shchelochkov O, Kelley B, Lee B (2010). Signaling pathways in human skeletal dysplasias. *Annu Rev Genom Hum G* 11; 189-217.
- Bale AE (2002). Hedgehog signaling and human disease. *Annu Rev Genom Hum G* 3; 47-65.
- Bandyopadhyay A, Yadav PS, Prashar P (2013). BMP signaling in development and diseases: a pharmacological perspective. *Biochem Pharmacol* 85; 857-864.
- Bilal M, Khan H, Khan MJ, Haack TB, Buchert R, Liaqat K, Ullah K, Ahmed S, Bharadwaj T, Acharya A, Peralta S (2023). Variants in EFCAB7 underlie nonsyndromic postaxial polydactyly. *Eur J Hum Genet* 31; 1270-1274.

- Bruckner P, van der Rest M (1994). Structure and function of cartilage collagens. *MRT* 28; 378-384.
- Bubshait DK (2022). A review of polydactyly and its inheritance: Connecting the dots. *Medicine* 101(50).
- Bulman MP, Kusumi K, Frayling TM, McKeown C, Garrett C, Lander ES, Krumlauf R, Hattersley AT, Ellard S, Turnpenny PD (2000). Mutations in the human delta homologue, *DLL3*, cause axial skeletal defects in spondylocostal dysostosis. *Nat Genet* 24; 438-441.
- Burger EB, Baas M, Hovius SER, Hoogeboom AJM, van Nieuwenhoven CA (2018). Preaxial polydactyly of the foot. *Acta Orthop* 89; 113–118.
- Caplan AI (1984). Cartilage. *SciAm* 251; 84-97.
- Castilla E, Paz J, Mutchinick O, Munoz E, Giorgiutti E, Gelman Z (1973). Polydactyly: a genetic study in South America. *Am J Hum Genet* 25; 405–412.
- Clarke B (2008). Normal bone anatomy and physiology. *Clin J Am Soc Nephrol* 3; S131.
- Comer GC, Potter M, Ladd AL (2018). Polydactyly of the Hand. *J Am Acad Orthop Surg* 26; 75-82.
- D'Angelo A, Franco B (2009). The dynamic cilium in human diseases. *Pathog* 2; 1-15.
- Da Silva JD, Tkachenko N, Soares AR (2023). Ellis-van Creveld Syndrome.
- Ehlen HW, Buelens LA, Vortkamp A (2006). Hedgehog signaling in skeletal development. *Birth Defects Research Part C: Embryo Today: Reviews* 78; 267-279.
- El-Ganzuri MA, Ahmed RR, Bastawy EM (2015). Regulatory mechanisms of bone development and function. *Int J* 3; 280-303.
- ELSavarirayan R, Rimoin DL (2002). The skeletal dysplasias. *Best Pract Res Clinic Endocrinol Metabol metabolism* 16; 547-560.
- Elsner J, Mensah MA, Holtgrewe M, Hertzberg J, Bigoni S, Busche A, Coutelier M, de Silva DC, Elçioglu N, Filges I, Gerkes E (2021). Genome sequencing in families with congenital limb malformations. *Hum Genet* 140;1229-1239.

- Fan L, Jin P, Qian Y, Shen G, Shen X, Dong M (2022). Case report: Prenatal diagnosis of postaxial polydactyly with Bi-allelic variants in smoothed (SMO). *Front Genet* 13; 887082.
- Farrugia MC, Calleja Agius J (2016). Polydactyly: a review. *Neonatal netw* 35; 135-142.
- Finley WH, Gustavson KH, Hall TM, Hurst DC, Barganier CM, Wiedmeyer JA (1994). Birth defects surveillance: Jefferson County, Alabama, and Uppsala County, Sweden. *South Med J* 87; 440-445.
- Florencio-Silva R, Sasso GR, Sasso-Cerri E, Simões MJ, Cerri PS (2015). Biology of bone tissue: structure, function, and factors that influence bone cells. *Biomed Res Int* 2015;1–17.
- Franz-Odendaal TA (2011). Induction and patterning of intramembranous bone. *Front Biosci* 16; 2734-2746.
- Furniss D, Critchley P, Giele H, Wilkie AO (2007). Nonsense-mediated decay and the molecular pathogenesis of mutations in SALL1 and GLI3. *Am J Med Genet A* 143; 3150-60.
- Furniss D, Critchley P, Giele H, Wilkie AOM (2007). Nonsense-mediated decay and the molecular pathogenesis of mutations in SALL1 and GLI3. *Am J Med Genet* 143A; 3150–3160
- Galjaard RJ, Smits A, Tuerlings JH, Bais AG, Avella AM, Breedveld G, Graaff ED, Oostra BA, Heutink P (2003). A new locus for postaxial polydactyly type A/B on chromosome 7q21–q34. *Eur J Hum Genet* 11; 409-415.
- Geister KA, Camper SA (2015). Advances in skeletal dysplasia genetics. *Annu Rev Genom Hum G* 16; 199.
- Girardi F, Le Grand F (2018). Wnt signaling in skeletal muscle development and regeneration. *PMBTS* 153; 157-179.
- Governale LS (2015). Craniosynostosis. *Pediatr Neurol* 53; 394-401.
- Graham TJ, Ress AM (1998). Finger polydactyly. *Hand Clin* 14; 49-64.
- Hadjidakis DJ, Androulakis II (2006). Bone remodeling. *Ann N Y Acad Sci* 1092; 385-396.
- Hartmann C (2007). Skeletal development are in control. *Mol. Cells*; 24; 177.

- Holmes LB, Nasri H, Hunt AT, Toufaily MH, Westgate MN (2018). Polydactyly, postaxial, type B. *Birth Defects Res* 110; 134–141.
- Huber C, Cormier-Daire V (2012). Ciliary disorder of the skeleton. *Am J Med Genet C: Semin Med Genet* (Vol. 160, No. 3, pp. 165-174). Hoboken: Wiley Subscription Services, Inc., A Wiley Company.
- Hurst JA, Firth HV, Smithson S (2005). Skeletal dysplasias. *Semin Fetal Neonatal Med* (Vol. 10, No. 3, pp. 233-241). WB Saunders.
- Ishigaki T, Akita S, Udagawa A, Suzuki H, Mitsukawa N (2021). Central polydactyly of the foot: An experience of a treatment of 22 patients. *J Orthop Sci*.
- Kannu P, Campos-Xavier AB, Hull D, Martinet D, Ballhausen D, Bonafé L (2013). Post-axial polydactyly type A2, overgrowth, and autistic traits associated with a chromosome 13q31.3 microduplication encompassing miR-17-92 and GPC5. *Eur J Med Genet*.56; 452-457.
- Kerchring T [1988]. “Spicilegium anatomicum continens observationum anatomicarum rariorum centuriam unam necnon osteogeniam foeruum etc,” in *Classification of Polydactyly of the Hands and Feet*, Vol. 107, eds W. Blauth and A. T. Olason [Amsterdam]. *Arch Orthop Trauma Surg* 334-34.
- Khan H, Ullah K, Jan A, Ali H, Ullah I, Ahmad WA (2023). A variant in the LDL receptor-related protein encoding gene LRP4 underlying polydactyly and phalangeal synostosis in a family of Pakistani origin. *Congenit Anom* 63; 190-194.
- Kornak U, Mundlos S (2003). Genetic disorders of the skeleton: a developmental approach. *AJHG* 73; 447-474.
- Krakow D, Rimoin DL. (2010). The skeletal dysplasias. *Genet Med* 12; 327-341.
- Kucheria K, Kenue RK, Taneja N (1981). An Indian family with postaxial polydactyly in four generations. *Clin Genet* 20; 36–39.
- Kucheria K, Kenue RK, Taneja N (1981). An Indian family with postaxial polydactyly in four generations. *Clin Genet* 20; 36-39.
- Kuroda Y, Kawai T, Goto K, Matsuda S (2019). Clinical application of injectable growth factor for bone regeneration: A systematic review. *Inflammation and regeneration* 39; 1-10.

- Kyriazis Z, Kollia P, Grivea I, Stefanou N, Sotiriou S, Dailiana Z (2023). Polydactyly: Clinical and molecular manifestations *World J Orthop*, 14; 13.
- Lange A, Müller GB (2017). Polydactyly in development, inheritance, and evolution. *Q Rev Biol* 92; 1-38.
- Lefebvre V, Bhattaram P (2010). Vertebrate skeletogenesis. *Curr Top Dev Biol* 90; 291-317.
- Lettice LA, Heaney SJ, Purdie LA, Li L, de Beer P, Oostra BA (2003). A long-range Shh enhancer regulates expression in the developing limb and fin and is associated with preaxial polydactyly. *Hum Mol Genet* 12; 1725–1735
- Lettice LA, Horikoshi T, Heaney SJ, van Baren MJ, van der Linde HC, Breedveld GJ (2002). Disruption of a long-range cis-acting regulator for Shh causes preaxial polydactyly. *Proc Natl Acad Sci* 99; 7548–7553.
- Lin W, Klein J (2021). Recent progress in cartilage lubrication. *Adv Mater* 33; 2005513.
- Liu F, Kohlmeier S, Wang CY (2008). Wnt signaling and skeletal development. *Cell Signal* 20; 999-1009.
- Lohan S, Spielmann M, Doelken SC, Flöttmann R, Muhammad F, Baig SM, Wajid M, Hülsemann W, Habenicht R, Kjaer KW, Patil SJ (2014). Microduplications encompassing the sonic hedgehog limb enhancer ZRS are associated with Haas-type polysyndactyly and Laurin-Sandrow syndrome. *Clin Genet* 86; 318-325.
- Lopez-Rios J (2016). The many lives of SHH in limb development and evolution. *Semin Cell Dev Biol* (Vol. 49, pp. 116-124). Academic Press.
- Malik S, Ullah S, Afzal M, Lal K, Haque S (2014). Clinical and descriptive genetic study of polydactyly in a Pakistani experience of 313 cases/families. *Clin Genet* 85; 482–486.
- Malik SA (2014). Polydactyly: phenotypes, genetics and classification. *Clin Genet* 85; 203-212.
- Mallo M (2020). The vertebrate tail: a gene playground for evolution. *CMLS* 77; 1021-1030.
- Mariani FV, Martin GR (2003). Deciphering skeletal patterning: clues from the limb. *Nature* 423; 319-325.
- Marie PJ, Miraoui H, Sévère N (2012). FGF/FGFR signaling in bone formation: progress and perspectives. *Growth Factors* 30; 117-123.

- Mellin GW (1963). "The frequency of birth defects," in Birth Defects, ed. M. Fishbein (Philadelphia, PA: JB Lippencott Co.); 1–17.
- Mohan J (1969). Postaxial polydactyly in three Indian families. *J Med Genet* 6; 196.
- Mortier GR (2001). The diagnosis of skeletal dysplasias: a multidisciplinary approach *Eur J Radiol* 40; 161-167.
- Mortier GR, Cohn DH, Cormier-Daire V, Hall C, Krakow D, Mundlos S, Nishimura G, Robertson S, Sangiorgi L, Savarirayan R, Silience D (2019). Nosology and classification of genetic skeletal disorders: 2019 revision. *Am J Med Genet A* 179; 2393-2419.
- Orioli IM, Castilla EE (1999). Thumb/hallux duplication and preaxial polydactyly type I. *Am J Med Genet* 82; 219-224.
- Ornitz DM, Marie PJ (2002). FGF signaling pathways in endochondral and intramembranous bone development and human genetic disease. *Genes Dev* 16;1446-1465.
- Palencia-Campos A, Ullah A, Nevado J, Yildirim R, Unal E, Ciorraga M, Barruz P, Chico L, Piceci-Sparascio F, Guida V, De Luca A (2017). *GLI1* inactivation is associated with developmental phenotypes overlapping with Ellis–van Creveld syndrome. *Hum Mol Genet* 26; 4556-4571.
- Perez-Lopez LM, Gutierrez-de la Iglesia D, Cabrera-Gonzalez M (2018). Radial Polydactyly. *Curr Pediatr Rev* 14; 91–96.
- Perez-Lopez LM, la Iglesia DG, Cabrera-Gonzalez M (2018). Radial polydactyly. *Curr Pediatr Rev* 14; 91-96.
- Radhakrishna U, Bornholdt D, Scott HS, Patel UC, Rossier C, Engel H (1999). The phenotypic spectrum of *GLI3* morphopathies includes autosomal dominant preaxial polydactyly type-IV and postaxial polydactyly type-A/B; No phenotype prediction from the position of *GLI3* mutations. *Am J Hum Genet* 65; 645–655.
- Rahim MC, Ali W, Samad A, Faiz S (2020). Clinical characterization of Post-axial Polydactyly. *Res J Adv Sci* 1.
- Rimoin DL, Cohn D, Krakow D, Wilcox W, Lachman RS, Alanay Y (2007). The skeletal dysplasias: clinical–molecular correlations. *Ann N Y Acad Sci* 1117; 302-309.

- Riobo NA, Saucy B, DiLizio C, Manning DR (2006). Activation of heterotrimeric G proteins by Smoothed. *Proc Natl Acad Sci* 103; 12607-12612.
- Rogers BH, Schmieg SL, Pehnke ME, Shah AS (2020). Evaluation and management of preaxial polydactyly. *Curr Rev Musculoskelet* 13; 545-551.
- Rohatgi R, Milenkovic L, Scott MP (2007). Patched1 regulates hedgehog signaling at the primary cilium. *Science* 317; 372-376.
- Salhotra A, Shah HN, Levi B, Longaker MT (2020). Mechanisms of bone development and repair. *Nat Rev Mol Cell Biol* 21; 696-711.
- Samarendra H, Wade RG, Glanvill L, Wormald J, Jain A (2022). Primary treatment of type B post-axial ulnar polydactyly: a systematic review and meta-analysis. *JPRAS open* 34; 21-33.
- Satake H, Ogino T, Takahara M, Kikuchi N, Muramatsu I, Muragaki Y, Kano H (2009). Occurrence of central polydactyly, syndactyly, and cleft hand in a single family: report of five hands in three cases. *J Hand Surg Am* 34; 1700-1703.
- Satir P, Christensen ST (2007). Overview of structure and function of mammalian cilia. *Annu Rev Physiol* 69; 377-400.
- Schramm T, Gloning KP, Minderer S, Daumer-Haas C, Hörtnagel K, Nerlich A, Tutschek B (2009). Prenatal sonographic diagnosis of skeletal dysplasias. (UOG): *Ultrasound Obstet Gynecol* 34; 160-170.
- Schrauwen I, Giese AP, Aziz A, Lafont DT, Chakchouk I, Santos-Cortez RL, Lee K, Acharya A, Khan FS, Ullah A, Nickerson DA (2019). FAM92A underlies nonsyndromic postaxial polydactyly in humans and an abnormal limb and digit skeletal phenotype in mice. *J Bone Miner Res* 34; 375-386.
- Su N, Du X, Chen L (2008). FGF signaling: its role in bone development and human skeleton diseases. (FBL) 13; 2842-2865.
- Swanson AB, Brown KS (1962). Hereditary triphalangeal thumb. *J Hered* 53; 259-265.
- Tada K, Kurisaki E, Yonenobu K, Tsuyuguchi Y, Kawai H (1982). Central polydactyly a review of 12 cases and their surgical treatment. *J Hand Surg Am*, 7; 460-465.

- Tang SJ, Hoodless PA, Lu Z, Breitman ML, McInnes RR, Wrana JL, Buchwald M (1998). The *Tlx-2* homeobox gene is a downstream target of BMP signalling and is required for mouse mesoderm development. *Development* 125; 1877-1887.
- Temtamy SA, McKusick VA (1978). "Syndactyly," in *The Genetics of Hand Malformations*. (New York, NY: Wiley); 301–322.
- Thioritz EW, Yurianto H, Saleh MR (2019). Isolated type II preaxial polydactyly with radial deviation of the terminal phalanges: A case report. *J Med Res* 9; 59–60.
- Thomas DC, Moorthy JD, Prabhakar V, Ajayakumar A, Pitchumani PK (2022). Role of primary cilia and Hedgehog signaling in craniofacial features of Ellis–van Creveld syndrome. *Am J Med Genet*. (Vol. 190, No. 1, pp. 36-46). Hoboken, USA: John Wiley & Sons, Inc.
- Tilemis FN, Marinakis NM, Kosma K, Fostira F, Traeger-Synodinos J (2023). Identification of a Novel IQCE Large Deletion through Copy Number Variant Analysis from Whole-Exome Sequencing Data of a Patient with Postaxial Polydactyly Type A7. *Mol Syndromol* 14; 225-230.
- Towers M, Wolpert L, Tickle C (2012). Gradients of signaling in the developing limb. *COCEBI* 24; 181-187.
- Tsai LP, Liao HM, Chen YJ, Fang JS, Chen CH (2009). A novel microdeletion at chromosome 2q31. 1-31.2 in a three-generation family presenting duplication of great toes with clinodactyly. *Clin Genet* 75; 449-456.
- Tsukurov O, Boehmer A, Flynn J, Nicolai JP, Hamel BC, Traill S (1994). A complex bilateral polysyndactyly disease locus maps to chromosome 7q36. *Nat Genet* 6; 282–286.
- Ullah A, Umair M, e-Kalsoom U, Shahzad S, Basit S, Ahmad W (2018). Exome sequencing revealed a novel nonsense variant in *ALX3* gene underlying frontorhiny. *J Hum Genet* 63; 97-100.
- Ullah I, Kakar N, Schrauwen I, Hussain S, Chakchouk I, Liaqat K, Acharya A, Wasif N, Santos-Cortez RL, Khan S, Aziz A (2019). Variants in *KIAA0825* underlie autosomal recessive postaxial polydactyly. *Hum Genet* 138; 593-600.
- Umair M, Ahmad F, Ahmad S, Alam Q, Rehan M, Alqosaibi AI, Alnamshan MM, Rafeeq MM, Haque S, Sain ZM, Ismail M (2021). A novel homozygous missense mutation in

- the zinc finger DNA binding domain of GLI1 causes recessive post-axial polydactyly. *Front Genet* 12; 746949.
- Umair M, Ahmad F, Bilal M, Ahmad W, Alfadhel M (2018). Clinical genetics of polydactyly: an updated review. *Front Genet* 9; 447.
- Umair M, Palander O, Bilal M, Almuzzaini B, Alam Q, Ahmad F, Younus M, Khan A, Waqas A, Rafeeq MM, Alfadhel M (2021). A biallelic variant in DACH1, encoding Dachshund Homolog 1, defines a novel candidate locus for recessive postaxial polydactyly type A. *Genom* 113; 2495-2502.
- Umair M, Shah K, Alhaddad B, Haack TB, Graf E, Strom TM, Meitinger T, Ahmad W (2017). Exome sequencing revealed a splice site variant in the IQCE gene underlying post-axial polydactyly type A restricted to the lower limb. *Eur J Hum Genet* 25; 960-965
- Unger S, Ferreira CR, Mortier GR, Ali H, Bertola DR, Calder A, Cohn DH, Cormier-Daire V, Girisha KM, Hall C, Krakow D (2023). Nosology of genetic skeletal disorders: 2023 revision. *Am J Med Genet A* 191; 1164-1209.
- van der Zwaag PA, Dijkhuizen T, Gerssen-Schoorl KB, Colijn AW, Broens PM, Flapper BC, van Ravenswaaij-Arts CM (2010). An interstitial duplication of chromosome 13q31.3q32.1 further delineates the critical region for postaxial polydactyly type A2. *Eur J Med Genet* 53; 45-49.
- Vargas-Franco D, Kalra R, Draper I, Pacak CA, Asakura A, Kang PB (2022). The Notch signaling pathway in skeletal muscle health and disease. *Muscle Nerve* 66; 530-544.
- Verma PK, El-Harouni AA (2015). Review of literature: genes related to postaxial polydactyly. *Front Pediatr* 3;8.
- Wan M, Cao X (2005). BMP signaling in skeletal development. *(BBRC)* 328; 651-657.
- Warman ML, Cormier-Daire V, Hall C, Krakow D, Lachman R, LeMerrer M, Mortier G, Mundlos S, Nishimura G, Rimoin DL, Robertson S. (2011). Nosology and classification of genetic skeletal disorders: 2010 revision. *Am J Med Genet A* 155; 943-968.
- Weldon SA, Münsterberg AE (2022). Somite development and regionalisation of the vertebral axial skeleton. *Semin Cell Dev Biol* (Vol. 127, pp. 10-16). Academic Press.

- Wellik DM (2007). Hox patterning of the vertebrate axial skeleton. *Dev Dyn De Dynam* 236; 2454-2463.
- Wieczorek D, Pawlik B, Li Y, Akarsu NA, Caliebe A, May KJ (2010). A specific mutation in the distant sonic hedgehog (SHH) cis-regulator (ZRS) causes Werner mesomelic syndrome (WMS) while complete ZRS duplications underlie Haas-type polysyndactyly and preaxial polydactyly (PPD) with or without the triphalangeal thumb. *Hum Mutat* 31; 81–89.
- Wieczorek D, Pawlik B, Li Y, Akarsu NA, Caliebe A, May KJ, Schweiger B, Vargas FR, Balci S, Gillessen-Kaesbach G, Wollnik B (2010). A specific mutation in the distant sonic hedgehog (SHH) cis-regulator (ZRS) causes Werner mesomelic syndrome (WMS) while complete ZRS duplications underlie Haas-type polysyndactyly and preaxial polydactyly (PPD) with or without triphalangeal thumb. *Hum Mutat* 31; 81-89.
- Wilkie AO, Morriss-Kay GM (2001). Genetics of craniofacial development and malformation *Nat Rev Genet* 2; 458-468.
- Williams S, Alkhatib B, Serra R (2019). Development of the axial skeleton and intervertebral disc. *Curr Top Dev Biol* 133; 49-90.
- Wood V (1970). Duplication of the index finger. *J Bone Joint Surg Am* 52; 569–573.
- Wood VE (1971). Treatment of central polydactyly. *Clin Orthop Relat Res* 74; 196-205.
- Xavier GM, Seppala M, Barrell W, Birjandi AA, Geoghegan F, Cobourne MT (2016). Hedgehog receptor function during craniofacial development. *Dev Biol* 415; 198-215.
- Xie Y, Su N, Yang J, Tan Q, Huang S, Jin M, Ni Z, Zhang B, Zhang D, Luo F, Chen H (2020). FGF/FGFR signaling in health and disease. *Signal Transduct Target Ther* 5; 181.
- Yamaguchi A, Ishizuya T, Kintou N, Wada Y, Katagiri T, Wozney JM, Rosen V, Yoshiki S (1996). Effects of BMP-2, BMP-4, and BMP-6 on osteoblastic differentiation of bone marrow-derived stromal cell lines, ST2 and MC3T3-G2/PA6. *(BBRC)* 220; 366-371.
- Zelzer E, Olsen BR (2003). The genetic basis for skeletal diseases. *Nature* 423; 343-348.
- Zhou GX, Dai L, Zhu J, Miao L, Wang YP, Liang J (2004). Epidemiological analysis of polydactylies in Chinese perinatal. *Sichuan Da Xue Xue Bao Yi Xue Ban* 35; 708–710

- Zhou H, Zhang L, Chen Y, Zhu CH, Chen FM, Li A (2022). Research progress on the hedgehog signaling pathway in regulating bone formation and homeostasis. *Cell Prolif* 55; e13162.
- Zieba JT, Chen YT, Lee BH, Bae Y (2020). Notch signaling in skeletal development, homeostasis, and pathogenesis. *Biomolecules* 10; 332.

ORIGINALITY REPORT

11%	6%	6%	3%
SIMILARITY INDEX	INTERNET SOURCES	PUBLICATIONS	STUDENT PAPERS

PRIMARY SOURCES

1	Submitted to Higher Education Commission Pakistan Student Paper	3%
2	www.ncbi.nlm.nih.gov Internet Source	2%
3	Zaheer Ahmad, Romana Liaqat, Oliva Palander, Muhammad Bilal, Shah Zeb, Farooq Ahmad, Muhammad Jawad Khan, Muhammad Umair. "Genetic Overview of Postaxial Polydactyly (PAP): Updated Classification", Clinical Genetics, 2022 Publication	1%
4	pr.hec.gov.pk Internet Source	1%
5	www.lajar.cl Internet Source	1%
6	Zisis Kyriazis, Panagoula Kollia, Ioanna Grivea, Nikolaos Stefanou, Sotirios Sotiriou, Zoe H Dailiana. "Polydactyly: Clinical and molecular	<1%


PROFESSOR
Department of Biochemistry
Quaid-i-Azam University, Islamabad